Design and Analysis for a 6u CubeSat and Mission -1

A Major Qualifying Project Report

Submitted to the Faculty of the

WORCESTER POLYTECHNIC INSTITUTE

in Partial Fulfillment of the Requirements for the

Degree of Bachelor of Science

in Aerospace Engineering

by

Philip Durgin

Veronika Karshina

Samuel Waring

March 18, 2022

Approved by: _____

Zachary R. Taillefer, Advisor

Assistant Professor, Aerospace Engineering Department,

WPI

Abstract

This paper presents the design of a scientific mission for a 6-unit CubeSat carrying a Gridded Retarding Ion Drift Sensor (GRIDS) and a Mini-Ion Neutral Mass Spectrometer (INMS) in order to measure particle composition in the F1 and F2 ionosphere layers. The CubeSat is inserted utilizing the Falcon 9 rideshare program at an altitude of 625km and transfers to a final semi-sun-synchronous orbit of 800km by 180km utilizing an NPT-30 I2 Ion Thruster. Propulsion analysis was conducted using MATLAB and STK in order to model orbital maneuvers and determine the total velocity budget. Mechanical design and analysis were done using SolidWorks and ANSYS. The constraints and requirements were determined based on the mission payload, Falcon 9 launch vehicle and Canisterized Satellite Dispenser. The Mechanical subsystem team was able to design a CubeSat that abided all the requirements set during the project. Power analysis was done using Systems Tool Kit (STK) and MATLAB. The requirements were that all subsystems needed to be powered for mission duration, and stored power was required for deorbit. A Helmholtz cage and air-bearing platform were developed and tested in order to simulate the magnetic environment encountered during Low Earth Orbit (LEO). This allowed for ground-based testing of the developed ADCS utilizing magnetorquers.

Acknowledgements

The team would like to thank the following individuals and groups for their help and support throughout the entirety of this project. Our primary and secondary advisors, Professor Taillefer, Gatsonis, and Demetriou have been instrumental in the success of this project. The team also would like to recognize the significant support received from Dr. Adriana Hera and Tina Stratis

Table of Authorship

Table of Contents

Table of Figures

Table of Tables

1. Introduction

This Major Qualifying Project (MQP) presents the analysis of the thermal and space environment aspects for the design of Appleton, a 6U CubeSat for an ionospheric science mission, and the continuing development of an attitude control and determination system (ACDS) test rig which includes a Helmholtz cage to simulate Earth's magnetic field at altitude and a low-friction platform to support magnetorquer-based testing of ADC components and systems. Appleton, shown in Figure 1, utilizes the NASA-designed miniature Ion Neutral Mass Spectrometer (mini-INMS) and Gridded Retarding Ion Drift Sensor (GRIDS) to measure the composition of the ionosphere's F layer.
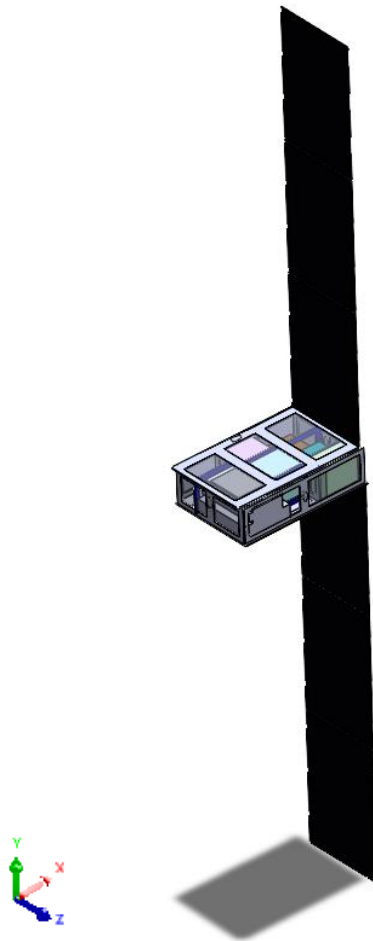
Figure 1: Appleton CubeSat with Solar Panels Deployed

The mission goal is to further the understanding of the ionosphere by analyzing its composition, local properties, and providing data to investigate any present anomalies. The CubeSat was given the name 'Appleton', after Sir Edward Victor Appleton, the physicist who won the Nobel Prize in physics for the discovery of the Ionosphere (Nobel Prize, 2022). Appleton operates in a semi-Sun-synchronous elliptical orbit with a perigee of 180 km and apogee of 600 km where it will collect data relevant to its mission objective.

This MQP group worked on the Appleton Project alongside partner MQP groups in the form of a Systems Engineering Group (SEG). The groups are referenced below according to the section they contributed to. The goals of the overall Appleton Project are to:

First, to design and ensure the functionality of Appleton for its mission duration of one year. The design was accomplished by the three MQP groups by addressing all the primary systems of the Appleton CubeSat that include mechanical (Karshina, et al., 2022), attitude determination and control (ADCS) (Gagnon, et al., 2022), telemetry and communication (Tierney, et al., 2022), command and data handling (Ritter, et al., 2022), power (Waring, et al., 2022), propulsion (Durgin, et al., 2022), payload integration (Lizotte, et al., 2022), thermal (Smith, et al., 2022), and environmental analysis (Lizotte, et al., 2022).

Second, to continue the design and development of a Helmholtz Cage for the testing of the ADCS subsystem. The cage will be designed to replicate the magnetic environment of a low Earth orbit, such that a test of Appleton's magnetorquer systems can be conducted.

1.1   Background and Literature Review

"Nano-satellite" refers to any satellite weighing between 1 and 10 kg and is a specification of CubeSats. Initially designed as low-cost test vehicles for satellite capabilities and design, CubeSats have slowly developed into cheap and low-weight satellites for military and scientific missions. In modern-day space applications, CubeSats are being used for a wide variety of research and communications missions and have undergone many design innovations. Typically, CubeSats operate in lower Earth orbit, which makes them ideal for

communications and atmospheric research purposes. CubeSats are typically sent into orbit via the upper stage of launch vehicles as auxiliary payloads. In recent years, NASA's CubeSat Launch Initiative (CSLI) has been working to provide more opportunities to send up satellites as secondary payloads on commercial or NGO launch craft.

Research into small satellite payload technology first began at WPI shortly after the advent of the CubeSat, with a 2001 MQP creating a balloon simulated satellite for a NASA sponsored educational program and a 2004 project studying magnetorquer attitude determination and control designs for small satellites. In the past decade WPI has significantly increased its research into CubeSats as costs have continued to drop and more institutions of higher education have started their own satellite programs. Since 2010, WPI has led several projects directed towards the study of CubeSats and their payload technology. These projects include investigations into CubeSat propulsion systems with various chemical propellants and experimental plasma propellants (A. Brown et al., 2021), (Lu, 2015), (Clavijo et al., 2020). Additionally, many early satellite MQPs researched the telecommunication and radar systems required for small low orbit satellites (A. Brown et al., 2021), (Olivieri, 2011), (Clavijo et al., 2020). In more recent years, WPI has conducted research and design into full satellite missions. The most recent projects have detailed auxiliary payload missions tasked with measuring the ionosphere through spinning and nadir fixed spacecraft like this project (A. Brown et al., 2021). In the future, WPI will continue to pursue CubeSat research including the potential development of a ground station on campus for more in-depth research opportunities.

1.2   Project Goals

The first goal of this MQP is to continue the series of CubeSat research projects done as part of the MQP program at WPI. This year the Appleton CubeSat mission will look to deliver the satellite to an elliptical semi-sun-synchronous orbit with a perigee of 180 km and an apogee of 800 km. Once this orbit is achieved, the scientific goal of the mission is to study the particle composition of the ionosphere using the two onboard payload sensors. The first is the Gridded Retarding Ion Drift Sensor (GRIDS) and the other is the Mini-Ion

Neutral Mass Spectrometer (Mini-INMS). These sensors can measure the situ density, velocity, temperature, and relative concentration of particles, which will be the focus of the data collected during the mission.

To complete the mission goals, efforts in designing spacecraft components and systems were split into eight subsystems. Each team member was responsible for designing one of the following subsystems: mechanical design and analysis, attitude determination and control, telemetry and communications, command and data handling, thermal, power, propulsion, space environment, and payload. The second goal of the project is to continue work by previous MQPs focusing on the design and testing of a Helmholtz cage. The Helmholtz cage can generate a dynamic magnetic field replicating that of Earth's own magnetic field. The development of this cage is crucial in testing the ADCS design, as Appleton will be affected by the Earth's magnetosphere during the duration of the mission. Therefore, it is important to determine all systems will be functional in this environment and demonstrate the effectiveness of magnetorquers in adjusting in the attitude of the spacecraft.

1.3   Project Design Requirements, Constrains and Other Considerations

This paper will cover the payload as well as the mechanical, power and propulsion subsystems. This paper's partner MQPs cover all other subsystems.

Subsystem Requirements:

Payload Requirements:

- The spacecraft shall be capable of assessing the local composition and state of the ionosphere.

Mechanical Requirements:

- The spacecraft design must be compatible with the launch vehicle
- The spacecraft design must be compatible with the Canisterized Satellite Dispenser (CSD).
- The spacecraft must be designed for the launch environment following the General Environmental Verification Standard (GEVS)

- The weight of the CubeSat will not exceed 9.1 kg

Attitude Determination and Control Requirements:

- The system shall maintain 3-axes of attitude knowledge better than 1 degree from apogee to perigee
- The satellite will successfully detumble, meaning it shall obtain negligible rotational velocity around at least two axes
- The spacecraft shall achieve sufficient torque authority to overcome predicted disturbance torques from gravity gradient, magnetic field, and thrust vector misalignment

Telemetry and Communication Requirements:

- The spacecraft shall have adequate data rate for command uplink over the entire range of altitudes.
- The spacecraft shall have adequate data rate to downlink science data stored.

Command and Data Handling Requirements:

- The spacecraft shall have the computational capability for closed loop ADC.
- The spacecraft shall have data capacity for science data.

Power Requirements:

- The telemetry, propulsion, payload, thermal and attitude control, must be powered for mission duration
- The spacecraft must be powered by a solar panel array and an onboard battery
- Stored power must be available for end of life deorbit

Propulsion Requirements:

- The thruster system shall be able to enter and maintain the scientific orbit with perigee of 180 km and apogee of 800 km.
- The thruster system shall be able to operate efficiently under power, mass, and volume constraints.

- The thruster shall be able to account for orbital perturbations.

Thermal Requirements:

- The spacecraft shall be designed to operate in an ambient and self-induced environment

- The thermal design shall provide temperatures within the following ranges: -20 C – 50 C

  Space Environment Requirements:

- The spacecraft shall be designed to operate for mission lifetime within the ambient and self-induced electromagnetic environment.

- The spacecraft shall be designed to operate for the mission lifetime within the ambient radiation environment.

- The spacecraft shall be designed to operate for the mission lifetime within the ambient micrometeorite and space debris environment.

  Helmholtz Requirements:

- The spacecraft's ADCS shall be validated through ground-based testing to within +/- 5° margin of error

- Generated magnetic fields will be measured and controlled; capable of reproducing expected field strengths for the orbit

- The test article must be attached to a torque-free rigging system, i.e., an air bearing platform

1.3.1 Design Constraints:
Payload Constraints:

- Both the Mini-Ion Neutral Mass Spectrometer (Mini-INMS) and Gridded Retarding Ion Drift Sensor (GRIDS) require RAM facing aperture orientation

- Total data collection rate of the payload is ~14 kbit/s, adequate data storage and transmission is required

- Functionality of the Mini-INMS ceases beyond the temperature range -10 to 50 °C

- Functionality of the GRIDS ceases beyond the temperature range -20 to 80 °C

- The payload requires a total power of 2.3 W for both devices

- The Mini-INMS and GRIDS require 1.3 U and 0.75 U of spacecraft volume, respectively

Space Environment Constraints:

- Environmental effects will be modeled to determine whether additional constraints will be added to the design

Power Constraints:

- Panels must point towards the sun at all times propulsion system is on

- Battery must maintain minimum temperature of –20 °C

Helmholtz Constraints:

- The Helmholtz cage must generate a reliable magnetic field in a volume large enough for a 6U test article to be placed (minimum 0.3 m^3)

- The air bearing platform must provide consistent pressure capable of lifting the test article allowing for torque-free rotation about the Z axis

1.3.2 Propulsion Constraints

Due to the imposed limitations of a 6U CubeSat design, the subsystem faces constraints on the amount of available volume and power reserved for propulsion systems. This affects decisions regarding the feasibility of thruster systems as well as placing limitations on the propellant mass available for burns throughout the mission's duration. Planned burns occur after deployment from the Falcon 9 launch vehicle, in which the CubeSat will be placed in an initial circular sun-synchronous parking orbit with an altitude of 500-600±25 km. In order to reach the final specified orbit of an 800 km apogee and a 180 km perigee, thrusters will be required

to perform two velocity-altering maneuvers. The first of two finite burns planned will enter the satellite into a transfer orbit, raising apogee altitude to 800 km. The second finite burn will lower periapsis altitude to 180 km, finalizing the planned scientific orbit for the remainder of the mission's duration.

The remaining propellant will be used for station-keeping in order to account for orbital perturbations associated with an orbit of this nature, extending the satellite's lifetime. The main perturbation that will need to be accounted for is drag, as the low perigee into the ionosphere will present a challenge when attempting to maintain the science orbit. Analysis of required scientific orbit and ΔV budget was conducted using MATLAB and the Systems Tool Kit (STK). This allowed for an estimation of the initial propellant mass value and therefore the amount of remaining propellant after achieving the desired orbit.

1.4 Project Management

For the duration of this MQP, the following subsystems were held:

- Mechanical Design (Veronika Karshina)

- Attitude Determination and Control (Jeremy Gagnon)

- Telemetry and Communication (Drake Tierney)

- Command and Data Handling (Christopher Ritter)

- Thermal (Harrison Smith)

- Power (Samuel Waring)

- Propulsion (Phillip Durgin)

- Space Environment (Tyler Lizotte)

During the first term of this MQP the team met each Tuesday to go over the weekly goals and then meet with the professor advisors Friday to go over mission objectives and what the team had accomplished during the week. To maintain order through the project the team appointed a project manager every three weeks; the main duties of the project manager included organizing weekly presentations, ensuring communication between each

subsystem, and updating the Gantt chart as needed. For the project budget the team was given $250 per student (totaling $2000) to use as needed.

1.5   MQP Objectives, Method and Standards

1. Develop Top Level Mission Objectives

    a. Evaluate the ionospheric composition between 180 km and 800 km.

    b. The spacecraft shall have a lifetime of 180 days

    c. The spacecraft shall occupy a polar, semi sun-synchronous orbit, at an inclination of 97.34 degrees

    d. At the end of life, the spacecraft shall enter a controlled deorbit

2. Scientific Objectives

    a. The spacecraft shall be capable of assessing the local composition and state of the ionosphere.

3. Payload Objectives

    a. The Mini-INMS shall remain functional for the mission duration and measure densities of neutral and ionized species in the ionosphere.

    b. The GRIDS shall remain functional for the mission duration and measure ion density, relative ion concentrations, temperatures, and velocity vectors (component normal to instrument face).

4. Orbital Objectives

    a. The spacecraft shall transfer from insertion to its final orbit.

    b. The spacecraft shall acquire a final sun-synchronous, elliptical, polar orbit with perigee of about 200 km and apogee about 800 km.

5. Mechanical Objectives

    a. The spacecraft design must be compatible with the launch vehicle.

    b. The weight of the CubeSat will not exceed 9.1 kg

     c. The spacecraft must be designed for the launch environment following the General Environmental Verification Standard (GEVS)

     d. The spacecraft design must be compatible with the Canisterized Satellite Dispenser (CSD).

     e. $- 50C$

6. Power Objectives

     a. Telemetry, propulsion, payload, thermal and attitude control, will be powered for mission duration

     b. System will be powered via solar panels and an onboard battery

     c. Stored power must be available for end of life contingency

7. Propulsion Objectives

     a. The thruster system shall be able to enter and maintain the scientific orbit with perigee of 180 km and apogee of 800 km

     b. The thruster system shall be able to operate efficiently under power, mass, and volume constraints

     c. The thruster shall be able to account for orbital perturbations

8. Helmholtz Cage

     a. The spacecraft's ADCS shall be validated through ground-based testing to within +/- 5° margin of error

     b. The Helmholtz cage shall be capable of recreating the magnetic environment the spacecraft shall experience

     c. The Air bearing platform shall be capable of producing the required air pressure to lift the test article

1.6   MQP Tasks and Timetable

During the first term of the project, the team followed the following Gantt Chart to remain on task throughout the project.
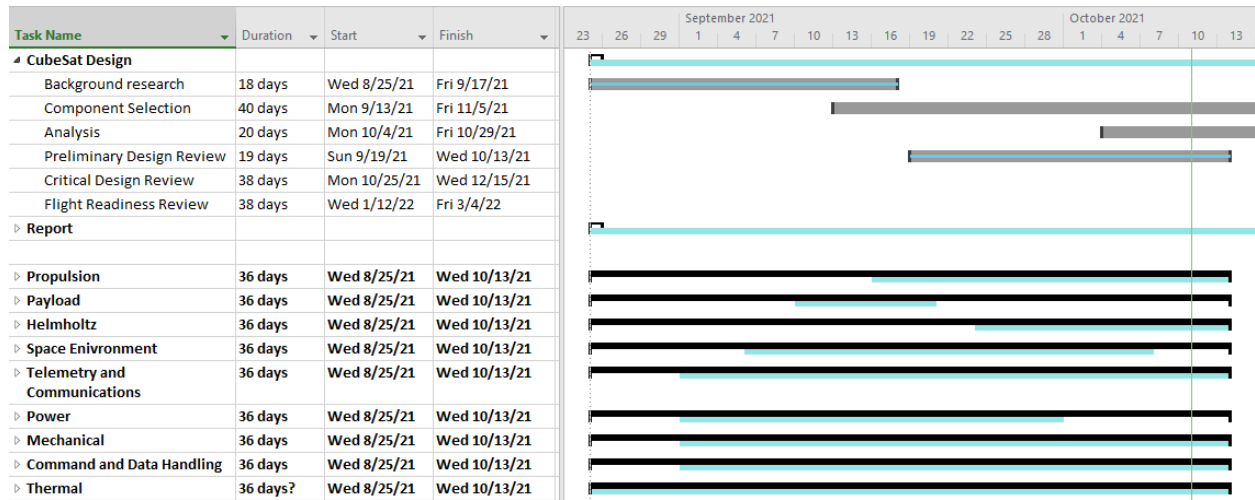
Figure 2: A Term Gantt Chart

1.7   Facilities and Equipment

The main facilities used for mission development were housed within Higgins Laboratory (HL) on the campus of Worcester Polytechnic Institute (WPI). Systems Engineering Group (SEG) meetings and subsystem team meetings, in which subsystem leads meet with their respective advisors. were conducted in-person and utilizing the video call application Zoom. The Helmholtz cage was stored within HL 016, with equipment required for testing provided by the WPI Aerospace Engineering Department. Software required for mission development and analysis, including Systems Tool Kit, MATLAB, and COMSOL, was made available through WPI owned licenses. Finally, training for this software was conducted in the Higgins Lab Design Studio as well as over Zoom.

2   Payload

The goal of this scientific mission is to interrogate the ionosphere across the F1 and F2 layers to collect data regarding the local composition and state of the ionic and neutral species. To accomplish this, two separate devices, the Mini-Ion Neutral Mass Spectrometer (Mini-INMS) and Gridded Retarding Ion Drift Sensor (GRIDS) were selected. Both instruments, when used in tandem, provide measurements of the densities of neutral and ionized species in the ionosphere, as well as relative ion concentrations, temperatures, and velocity vectors (component normal to instrument face).

2.1   Mini-Ion Neutral Mass Spectrometer (INMS)

NASA Goddard's Mini-INMS can provide in situ density measurements of ion and neutral species in the ionosphere. Specifically, it can measure densities of the species shown in Table 1.

Table 1: Parameters and Performance of the Mini-INMS (J. Klenzing et al., 2019), (M. Rodriguez et al., 2016)

Parameter	Performance
Ion Species	H^+, He^+, N^+, O^+, NO^+, O_2^+
Ion Range	$10^3 \, cm^{-3}$ to $10^7 \, cm^{-3}$
Neutral Species	H, He, N, O, N_2, O_2
Neutral Range	$10^5 \, cm^{-3}$ to $10^9 \, cm^{-3}$
Volume	1.3 U
Mass	960 g
Power	1.8 W
Cadence	1 s
Data Rate	13.1 kbit/s
Operating Temperature	-10 to 50 °C
FOV	$\pm 20°$ x $\pm 10°$ around ram

The Mini-INMS measures these densities using a gated time-of-flight (TOF) instrument as shown in Figure 3. Both the neutral and ion apertures use this instrument to measure the mass of each species according to their TOF.
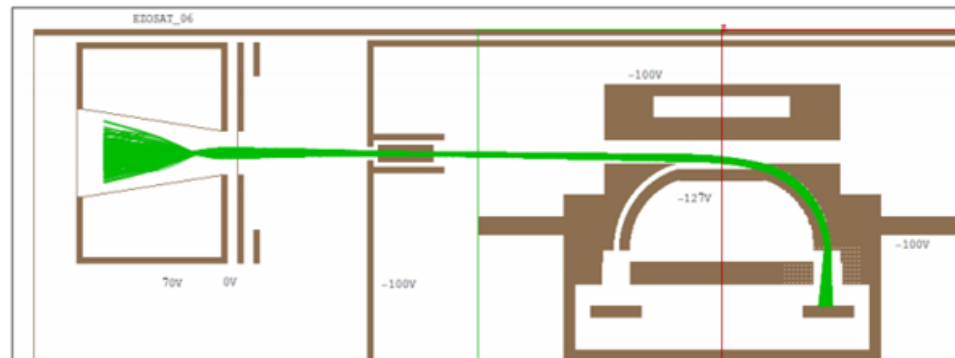
Figure 3: Gared Time-of-Flight (TOF) Apparatus (M. Rodriguez et al., 2016)

On the ion side, particles enter the aperture and receive a pre-acceleration voltage which gives all ions essentially the same energy. While the energy of incoming ions will vary, the voltage applied is orders of magnitude greater, thereby negating this difference. With all ions having the same kinetic energy their velocity into the instrument will be solely dependent on the particle mass; heavier ions will travel more slowly than lighter ions. The faster moving ions will have a lower time of flight (TOF) than heavier ions; by ordering ions in their velocity according to their mass a TOF model can be created for the collection period, as shown in Figure 4.
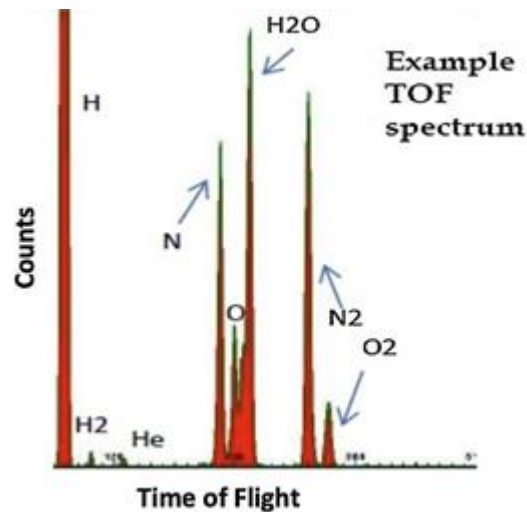
Figure 4: Counts of Detected Masses According to Their TOF (M. Rodriguez et al., 2016)

Similarly, on the neutral side, particles are also given an initial pre-acceleration voltage to use the same

TOF methods as on the ion side. The main difference between the two is that the neutral side also contains an

ion repellant at the aperture to only allow neutral particles entry. In this way the densities of both the ionized

and neutral species can be measured. The entire apparatus is shown in Figure 5.
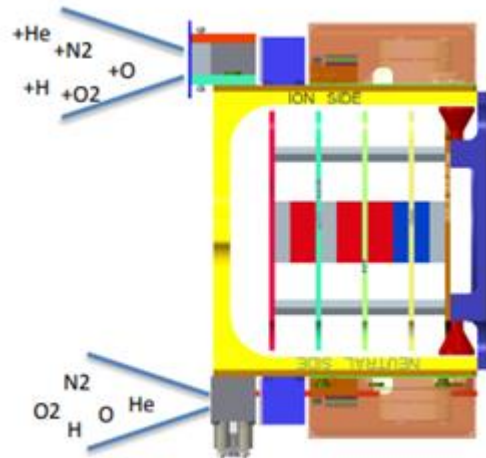
Figure 5: The Mini-INMS Species Collection System (M. Rodriguez et al., 2016)

The functionality of the INMS has been proven in multiple missions including ExoCube, Dellingr, and petitSat.

The ExoCube, flown in 2015, was the first flight of the Mini-INMS. However, due to inadequate antenna

deployment on the CubeSat the data received was less than desired. The instrument functioned well and was

able to send TOF spectrums that aligned with those predicted, such as the sample shown in Figure 4, but ultimately communication with the CubeSat was lost (M. Rodriguez et al., 2016). Unfortunate circumstances also occurred with the NASA Dellingr spacecraft, launched in 2017. The CubeSat was accidentally powered before deployment resulting in a dead battery from the start of the mission (M. Hatfield, 2018). While the CubeSat was able to recover using its solar panels. After the completion of outgassing the remaining particles left in the INMS from Earth's atmosphere the satellite was able to successfully activate and record data from the ion side of the INMS as shown in Figure 6. Data from the neutral side of the INMS has not been able to be demonstrated by this mission.
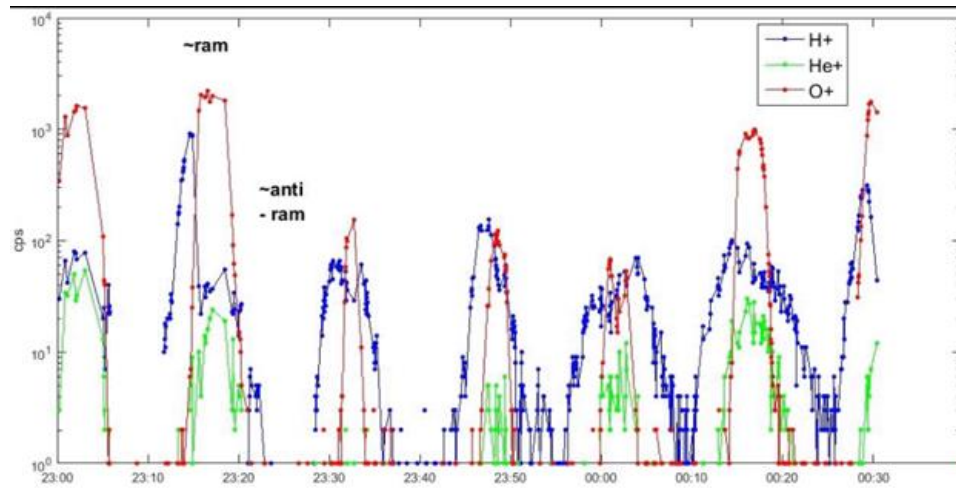
Figure 6: Initial Ion Measurements from the INMS aboard NASA Dellingr (M. Hatfield, 2018)

2.2 Gridded Retarding Ion Drift Sensor (GRIDS)

The GRIDS system can provide in situ ion density, temperature, relative concentration of

heavy to light ions, and the component of the velocity vector normal to the instrument face. Specifically, it can measure the parameters shown in Table 2.

Table 2: Parameters and Performance of the Mini-INMS (M. Rodriguez et al., 2016), (Davidson et al., 2020)

Parameter	Performance
Velocity Range (Accuracy)	-1500 m/s to 1500 m/s ($\pm$10 m/s)

Ion Species	H^+, He^+, O^+
Ion Density Range (Accuracy)	5×10^3 cm^{-3} to 5×10^7 cm^{-3} (500 cm^{-3} or 2%)
Ion Temperature Range (Accuracy)	0 K to 3000 K (10 K or 5%)
Ion Composition Range (Accuracy)	0 to 1 (0.02)
Volume	0.75 U
Mass	500 g
Power	0.5 W
Cadence	0.5 Hz
Data Rate	533 bit/s
Operating Temperature	-20 to 80 °C

The GRIDS device is made of a series of biased and grounded grids located behind a RAM facing aperture. These grids are supplied with a retarding voltage to act as ion-energy filters (M. Hatfield, 2018). At the back of the instrument there are ion collectors which detect currents produced from ion impacts. By varying the retarding voltage in the aperture grids the ion species can be selectively allowed to pass through and into the collectors. Current from ions impacting the collector is used to calculate total ion flux as a function of retarding voltage (M. Hatfield, 2018). From this calculation the ion density, temperature, relative concentration of heavy to light ions, and the component of the velocity vector normal to the instrument face can be derived. The grids sensor and the breakdown of its internal grids are shown in Figure 7 and Figure 8.
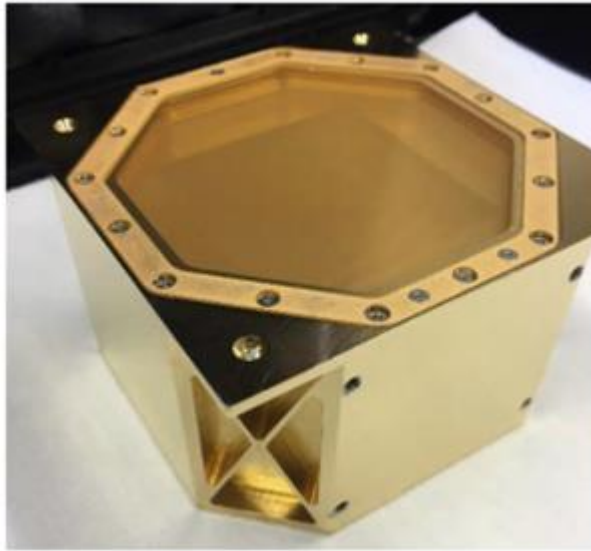
Figure 7: The GRIDS apparatus

Aperture Grid
Light-Ion Rejection Grid
Square Collimator
Retarding Grid
Electron Suppression Grid
Segmented Collector

Four-Channel Electrometer

Control Electronics
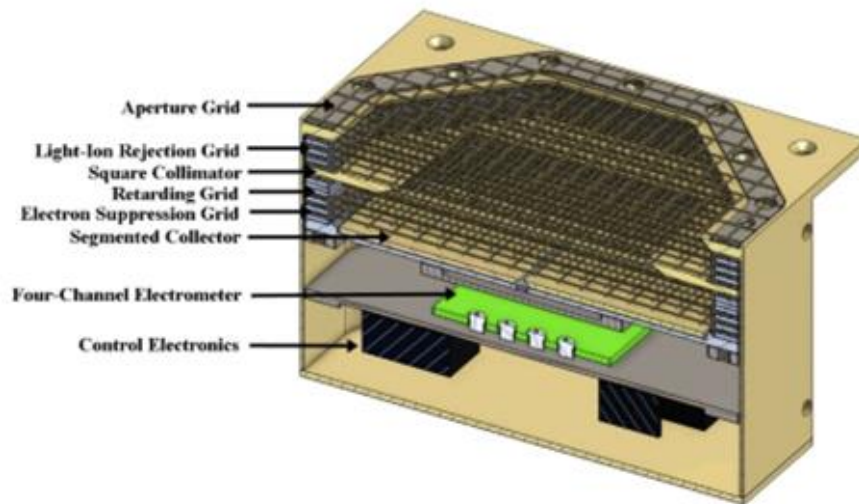
Figure 8: Grids within the GRIDS system

The GRIDS system and the Mini-INMS were both selected for the petitSat mission, deploying from the ISS in 2021, this mission will help determine the link between plasma enhancements and medium-sized traveling ionospheric disturbances (MSTIDs) (L. Keesey, 2017).

3 Mechanical Design and Analysis

The Mechanical Design subsystem is responsible for creating the design of the CubeSat that contains all the components necessary for the mission and abides the requirements for the satellite dispenser and launch

vehicle. The Mechanical Design subsystem is also responsible for performing simulations and tests to ensure the satellite can survive launch conditions and remain mechanically sound, however, in this project the focus is purely on computer-aided analysis with no further testing. This section of the report discusses the mechanical design and subsequent mechanical analysis of the Appleton Nano-Sat, as well as the selection of the satellite dispenser and the launch vehicle.

3.1 Launch Vehicle and Satellite Dispenser selection

3.1.1 Satellite Dispenser Selection

During launch, prior to mission the CubeSat is contained within a satellite dispenser that attaches to the launch vehicle. The dispenser has a spring-loaded door on one side that activates and dispenses the satellite at the desired altitude (J Puig -Suari & R Nugent, 2015). There are two types of CubeSat dispensers. Both dispense the vehicle using a spring-loaded pushing plate, the difference is how the satellite is secured within the dispenser.

The first method, used in Tyvak and Innovative Solutions In Space (ISIS) dispensers, is four rails at each corner of the satellite Figure 9. The rail dispenser provides extra insulation between the payload and the outer part of the dispenser, the insulators are located in the 0.5 mm gap between the rails and the outer wall. In this configuration the payload might vibrate making it difficult to model accurately.
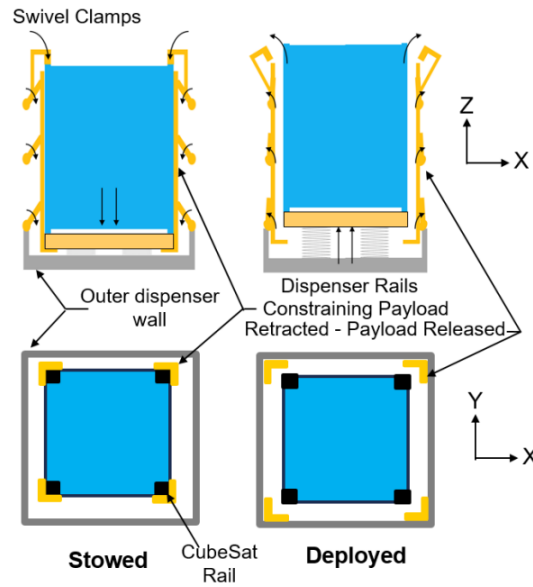
Figure 9*: Rail CubeSat Dispenser* (J. Carnahan & A. Kruggel, 2018)

The second method, used in Planetary Systems Corporation dispensers, is using two thinner rails or tabs, that are clamped to the dispenser Figure 10. Tabs provide a secure connection between the payload and the dispenser allowing for accurate modelling of the systems responses to vibrations and loading. The MQP project is focused on the design of the satellite, therefore it is important to have accurate predictions using software. For the project Canisterized Satellite Dispenser (CSD) with tabs was chosen. In addition, payload specifications for the Planetary Systems Corporation (PSC) dispenser were available online, which made it easier to follow requirements when modelling.
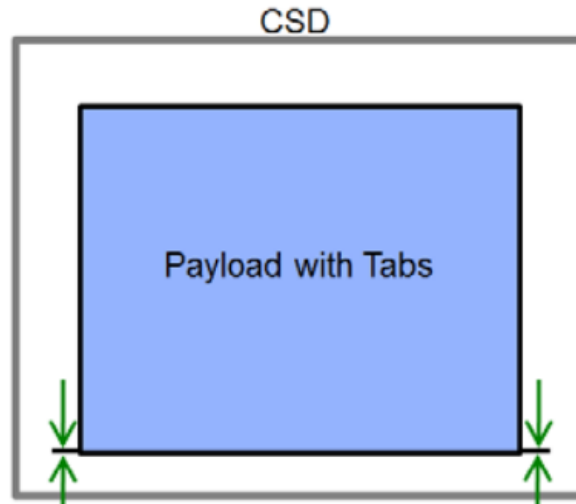
Figure 10: Tabs CubeSat Dispenser (Planetary Systems Corporation, 2020)

Once the satellite dispenser was chosen several constraints were applied to the design. CSD is a standard unit that is manufactured by PSC, therefore, the payload must follow the requirements provided in the Payload Specification(Planetary Systems Corporation, 2020). There is around 389.56 cm^3 volume that the CubeSat can occupy, there is a 9.1 kg maximum mass limit, constraints on the location of the center of mass and the maximum tab loading cannot exceed 3559 N. Further break down of these requirements and their effects on the design can be found in section 3.2 Mechanical Requirements.

3.1.2 Launch Vehicle Selection

There have been 19 missions where CSD was used to dispense CubeSatellites, from these missions several launch vehicles could be identified that are proven to be compatible with this system: Electron (6 missions), Falcon 9 (5 missions), Atlas 5 (3 missions), SPARK (1 mission), Minotaur IV (1 mission), PSLV-CA (1 mission), LauncherOne (1 mission) and Antares (1 mission). Due to the requirements of the mission orbit, as well as the availability and accessibility of information, SpaceX's Falcon 9 rocket was chosen as the primary launch vehicle. Appleton will utilize the SmallSat Rideshare program and be attached to a mechanical interface rig.

The Falcon 9 rocket will eject the CubeSat into an initial parking orbit with an apogee and perigee of approximately 500 to 600 kilometers. The orbit will share the inclination of the final orbit, with a value of 97.34 degrees. This will allow Appleton to be sun-synchronous, meaning that the spacecraft will process with the same period as Earth's solar orbit. This is optimal as the CubeSat will need to be sun-facing in order to optimize power generation.

3.2   Mechanical Requirements

The mechanical requirements section discusses requirements that are imposed on the design by factors not related to the team's mission goals, such as maximum satellite dispenser limitations and regulations in the launch vehicle manual. A list of requirements compiled from these documents is below:

CSD requirements (Planetary Systems Corporation, 2020):

- Tabs shall be aluminum alloy with yield strength ≥56ksi.

- Tab load will not exceed 3559 N.

- Maximum stress should not exceed 503 MPa.

- Holes, countersinks, and any protruding features are prohibited anywhere along the Tabs.

- Tabs shall be Hard Anodized per MIL-A-8625, Type III, Class 1. All dimensions apply after hard anodize.

- Max surface roughness is N7 (1.6 μm Ra, 63 μin AA).

- By default, tabs shall run the entire length of the payload. Gaps are allowed and are defined in the manual; however, the allowable maximum load and payload mass must decrease accordingly.

- Dimensions and tolerances shall be maintained under all temperatures. Temperatures experienced by the payload can be generated based on the maximum fairing temperature graph found in the Falcon 9 rideshare manual (Space X, 2021).

- The structure comprising one of the 2U × 1U faces (that contacts CSD ejection plate) may be a uniform surface or consist of discrete contact points. The discrete contact points shall be located such that they envelope the payload's center of mass and any deployment switches.

- Safe/Arm plug, if necessary, shall reside in specified zone on 2U × 1U face opposite to ejection plate (preferred) or either of the 3U × 1U faces.

- No debris shall be generated that will inhibit separation.

- Mass shall not exceed 9.1 kg.

- For the solar panels ensure sufficient CSD contact spacing and panel stiffness to prevent the panel from rubbing on the dispenser as the payload ejects.

- Deployables should have features to react shear loading at end opposite hinge.

- The deployable panels shall be sufficiently preloaded against the payload structure to minimize rattling during launch.

The dimensions of the CubeSat are determined based on the available space inside the CSD called the dynamic envelope.

Maximum dynamic envelope (Planetary Systems Corporation, 2020)

- Center of mass in a stowed CSD configuration will be located (see Figure 11 for coordinate system):
- x-direction: between -40 and 40 mm
- y-direction: between 10 and 70 mm
- z-direction: between 133 and 233 mm
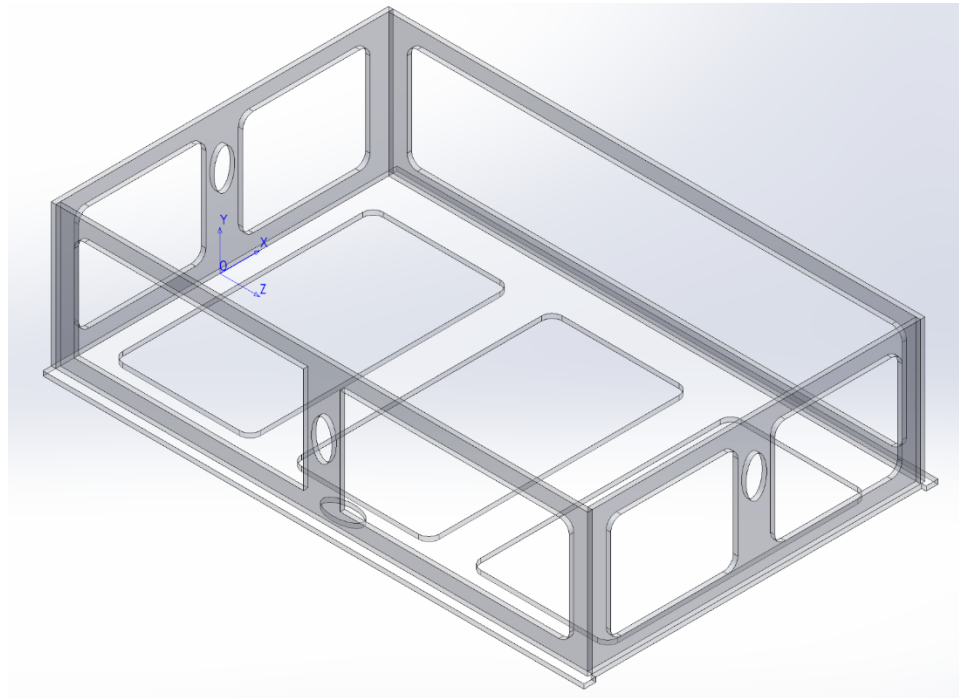
Figure 11: Coordinate system used to describe dynamic envelope requirements. The origin is located on the face coincident with the ejection plate.

- Maximum height (y-direction): 109.7 mm

- Maximum/tab width (x-direction): 239.4 mm

- Maximum/tab length (z-direction): 366 mm

- Maximum deformation shall not exceed the dimensions of the CSD

  Falcon 9 requirements (Space X, 2021):

- Payload's fundamental frequency must exceed 40 Hz.

- Payload shall meet random vibration requirements stated in the manual.

- Non-metallic materials used in payload must not exceed mass loss of 1%.

- Payload will undergo all required verification testing (shock, random vibration, static load, pressure systems, electromagnetic compatibility).

3.3 Mechanical design

The first step in designing the Appleton Nano-Sat was determining the requirements that the design must follow; these requirements can be found in Section 3.2. Based on the satellite dispenser choice the maximum dimensions of the dynamic envelope were modeled. This model is shown in Figure 12, the maximum dimensions for the dynamic envelope allow for 10090 cm^3 of usable volume.
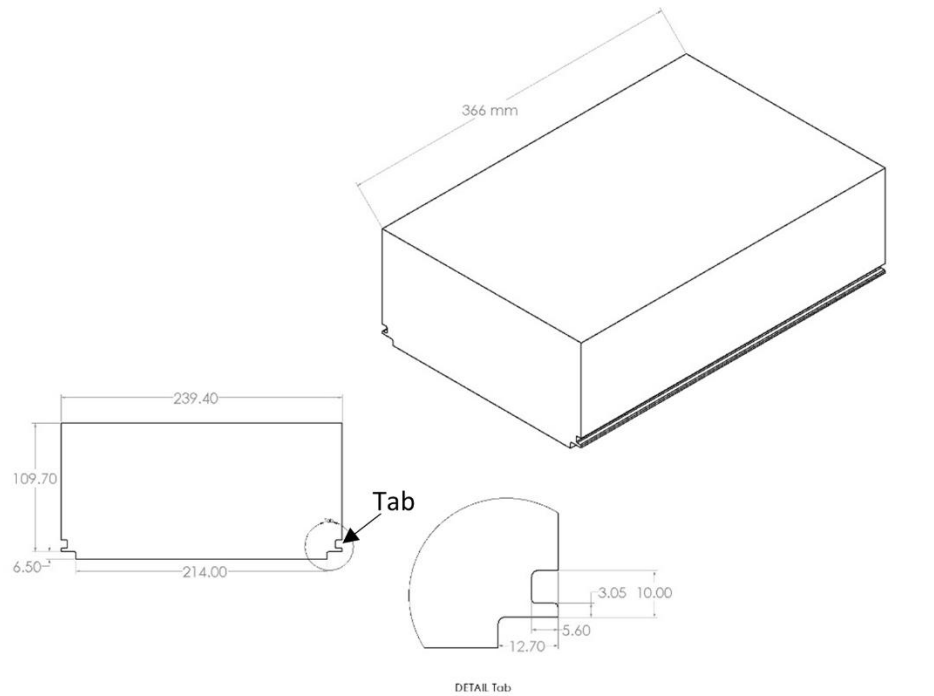
Figure 12: Maximum CubeSat dimensions.

Next, from a mechanical design perspective, power needs were considered. The spacecraft will require most power during orbital transfer and the scientific mission, power requirements are discussed in detail in Section 8. To accommodate the power subsystem, it was decided to have folding solar panels that will be stowed during launch. One solar panel will occupy the 6 mm × 214 mm × 366 mm pocket under the tabs and the second will be stowed on the "top" 3U × 2U face, reducing available height of the dynamic envelope.

The orientation of the spacecraft in orbit significantly affects the placement of certain components, including the payload, solar arrays, sun sensors and others. It was decided to have a 3U × 1U side be RAM-

facing (or perpendicular to the velocity vector in the direction of motion), for both payloads to fit and be able to collect data. The sensors of both mini-INMS and GRIDS needed to be placed against the RAM face, therefore, the additional 5.6 mm on each side of the 2U × 1U faces were reduced, so that the 3U × 1U wall became flat from tabs up to the top surface. This left 7600 cm^3 of usable volume. (Figure 13)
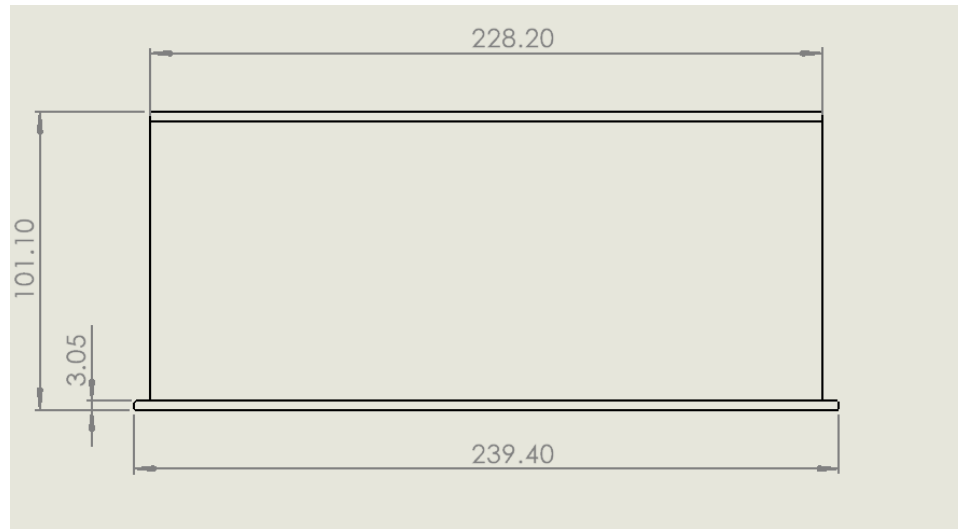
Figure 13: Appleton Nano-Sat dynamic envelope dimensions (mm)

The next step of the mechanical design is placing internal components and meeting requirements for placement of each one. The dimensions and requirements for each component are listed in Table 3 below:

Table 3: List of component dimensions, mass and placement requirements

Component Name	Dimensions	Mass	Requirement(s)
ADCS	96.9 x 90.5 x 85mm	880 g	Close to the center of mass
Battery	95.84 × 90.17 × 27.35 mm	335 g	
Computer	95.89x90.17x5.51 mm	6.19 g	
GRIDS	95 × 95 × 54 mm	509 g	RAM facing
INMS	Figure 14	600 g	RAM facing
Patch Antenna	70 x 70 x 3.4 mm	49 g	Earth-facing
Propulsion system	96 x 96 x 113 mm	1200 g	Opposite to RAM
Solar Sensors	27.4 × 14 × 5.9 mm	4 g	One on 5 sides
Transceiver	50x55x94 mm	275 g	Needs access to the patch antenna
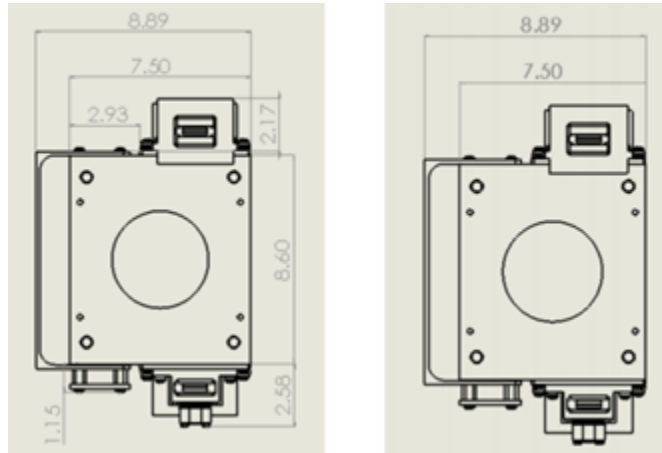
Figure 14: Dimensions of the mini-INMS (cm).

The two sensors (mini-INMS and GRIDS) were placed first on the RAM-facing side at opposing ends and governed the placement of surrounding components. The two sensors split the body of the satellite into three relatively even sections. Two long internal brackets were modeled to outline these sections. Components are secured to the frame of the CubeSat via smaller brackets that are bolted in between the long internal brackets and the sides of the CubeSat.

Next, the propulsion subsystem was placed in the middle section against the anti-RAM side. The ADCS was placed in the middle section next to the propulsion to be located as near as possible to the center of mass. The patch antenna (not visible in Figure 15) is located on the nadir side at the center of the tab plate. The transceiver was placed behind GRIDS to have easy access to the patch antenna. Approximately 1U of space in the "right" section (closest to the sun-facing side) of the CubeSat was left for additional electronics and wiring. The battery was placed in that segment since a lot of the wires will be attached to it. The empty space towards anti-RAM from the mini-INMS is also reserved for electronics and wires since that is where the on-board computer is located. Small cut-outs were made on each side but the anti-RAM to place the five sun sensors. The overall layout of the components can be seen in Figure 15.

ADCS
Battery
Computer
GRIDS
mini-INMS
Propulsion Sybsystem
Solar Sensors
Transciever
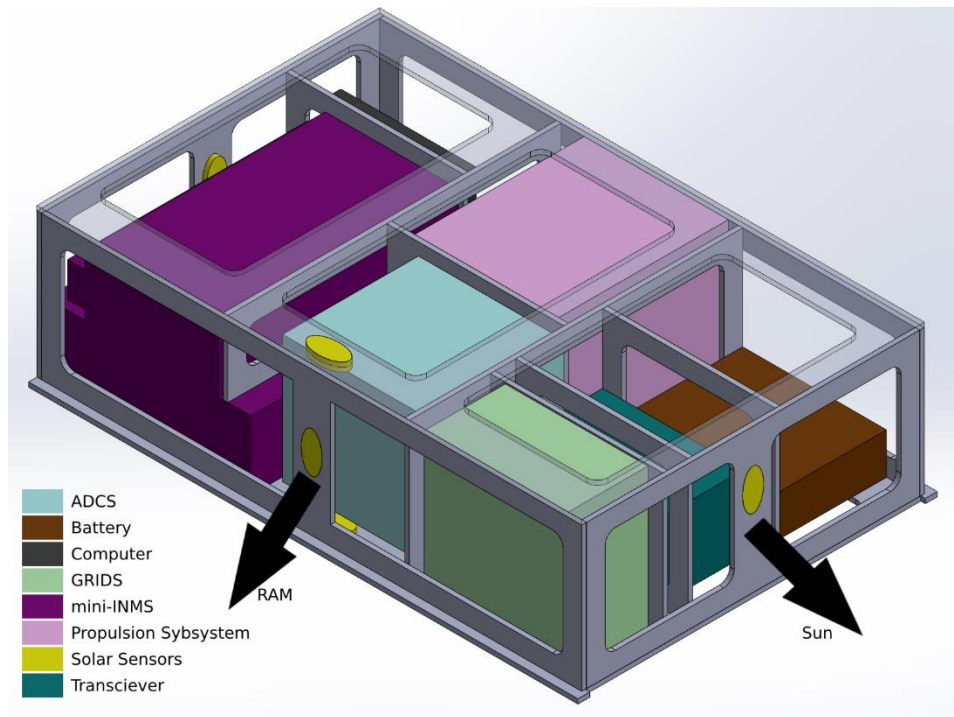
Figure 15: Appleton Nano-Sat configuration

As for the overall structure of the CubeSat it was modified to reduce weight. The thickness for the structural components was set to 3.05 mm to be uniform with the tabs. Cut outs were made on all sides, the brackets were also designed hollow (Figure 16). The original solid structure weighed over 2.5 kg, the redesign weighed 1289.28 grams and still met all the requirements as will be demonstrated in Section 3.4 Mechanical Analysis.

To ensure temperature control and radiation protection the CubeSat requires a 0.5 mm layer of multi-layer insulation (MLI) to cover all the openings in the structure. The only parts not covered by it are the fields of view of the sensors, the patch antenna on the nadir side and the propulsion subsystem. The outside design of the Appleton Nano-Sat excluding the solar panels and showing the min-INMS and GRIDS fields of view can be found in Figure 17.
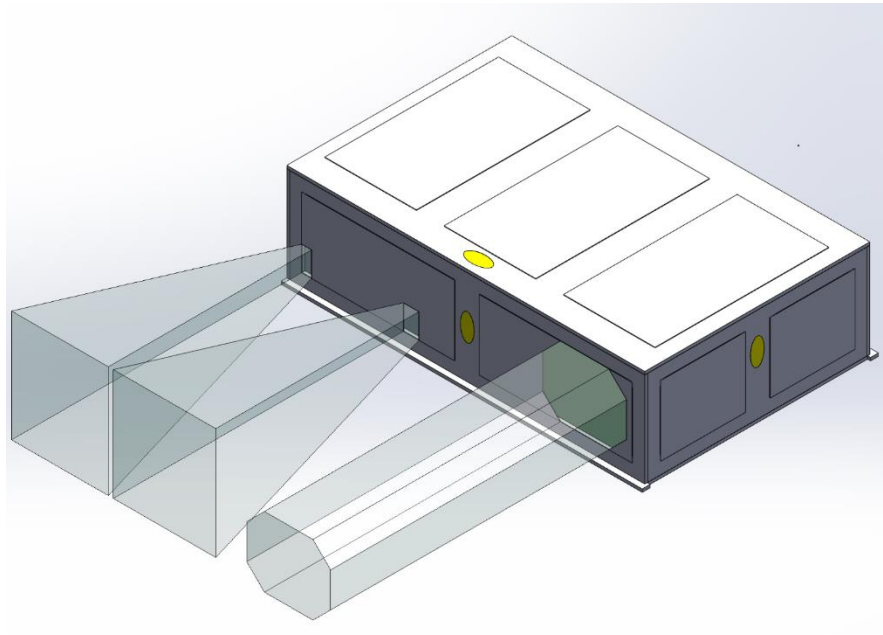
Figure 17: Final design of the CubeSat with modelled fields of view.

As mentioned earlier the solar panels are stored folded under the tab and on top of the CubeSat. Each solar panel is $3U \times 2U$ and there are six solar panels (3 at the bottom and 3 on top), so the overall area is roughly 36U. The solar panel design was inspired by DMSA: Deployable Multifunction Solar Array, which are flight proven and were featured in the NASA state of the art review (Caldwell, 2021). In Appleton NanoSat design thin (2 mm including structure) solar panels are stacked on top of each other and are connected via spring loaded hinges. Similarly, to the DMSA a release control board, stored in the electronics bay above the battery, will control the spring-loaded release mechanism. The stowed and deployed configuration of the solar panels can be found in Figure 18.
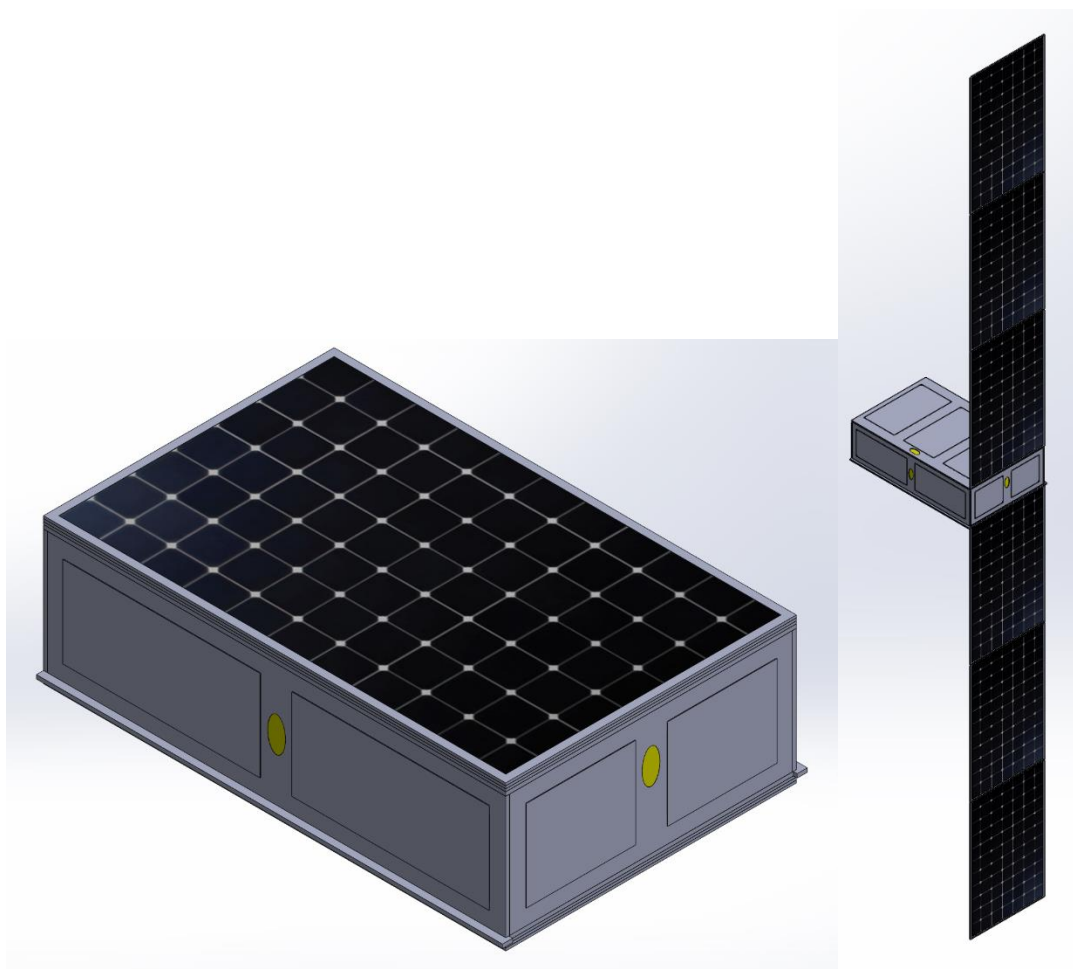
Figure 18: Stowed (left) and deployed (right) solar panel configurations.

3.4   Mechanical Analysis

Before describing the mechanical analysis, below is a summary of parameters that were checked in order
to ensure the design meets the requirements established in Section 3.2:

- Total mass

- Center of mass

- Natural frequencies

- Loading on the tabs response to random vibration specters provided by SpaceX (Space X, 2021)
  and NASA (NASA, 2019)

- Deformation after the random vibration analysis

- Maximum stress in the structure

Finding the total mass and the center of mass can be done in SolidWorks, where the satellite was modeled in the Mass Properties section. The final wet mass including solar panels and the MLI is 6010.71 grams, which is within the 9.1 kg limit set by the CSD. The center of mass also falls within the allowed and is located at:

- X = 4.09 mm (required between –40 and 40 mm)

- Y = 46.29 mm (required between 10 and 70 mm)

- Z = 196.24 mm (required between 133 and 233 mm)

ANSYS was used to perform random vibration analysis. The ANSYS workbench set up can be seen in Figure 21 and is discussed in depth in the section below. Before conducting analysis in ANSYS a mesh must be created. When using ANSYS the geometry should be simplified, if possible, since most components were already assumed to be uniform cubes little further simplification was required. The MLI covers were removed since they are thin foil and would not affect the performance of the structure. Due to the thinness of the solar panels and the fact that they were stacked on top of each other, the layers and connections in the simulation were overlapping and it was decided to remove them, since they are an attachment to the structure rather than part of it. Then the geometry was imported into ANSYS from SolidWorks and each component was assigned a custom material based on densities known from the original model. Aluminum alloy was assigned to the structure and brackets.

The smallest thickness in the design is 3.05 mm, so that seemed like a reasonable size for the mesh elements, however when running the simulation, it became apparent that it was taking too long (over 20 minutes). Next, 4 mm mesh was considered, simulations with that mesh were taking 15 minutes to converge, which seemed unreasonable for testing multiple designs in a reasonable time. Increasing the size of the mesh elements leads to a decrease in accuracy and overall quality of the mesh, before selecting an even larger mesh

these parameters were considered. Below in Table 4 is data on the quality of the 4 mm, 5 mm and 6 mm mesh can be found:

Table 4: Characteristics of several ANSYS meshes of the model

	4 mm	5 mm	6 mm
Average Element Quality	0.98915	0.97027	0.95264
Average Aspect Ratio	1.091	1.1791	1.246
Simulation Run Time	15 minutes	7 minutes	4 minutes

An ideal mesh has element quality and aspect ratio of 1. As evident from Table 4 the respective numbers are getting further from 1 as the element size increases. Both 5 mm and 6 mm meshes are of acceptable quality, since the time given to complete the project allowed for it a 5 mm mesh was chosen for more accuracy in reasonable time. Figure 19 shows the chosen mesh.
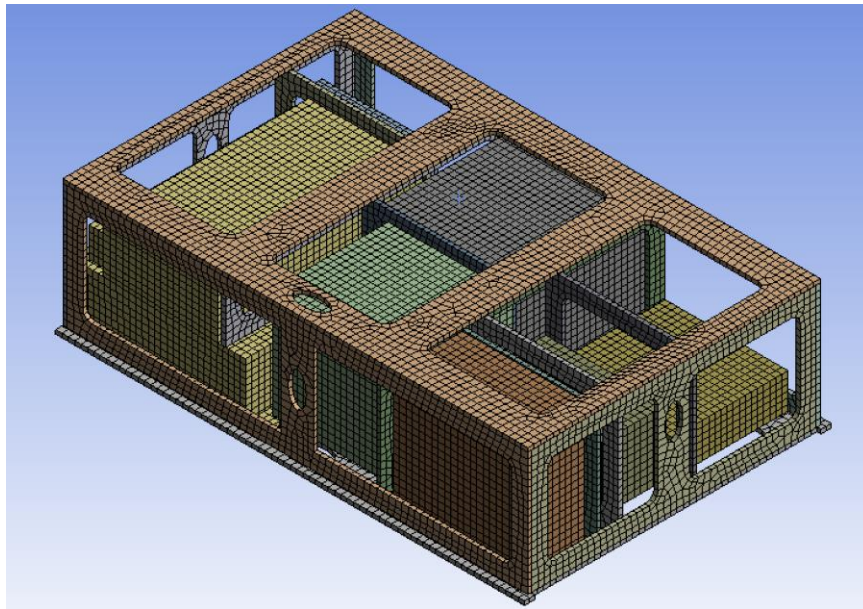
Figure 19: Mesh used in ANSYS analysis.

First Static Structural Analysis was performed to add the acceleration due to gravity and the fixed supports on the faces of the tabs facing RAM and anti-RAM directions. These fixed supports simulate the clamping of the satellite inside the CSD. Next, the results of the Static Structural analysis were passed to the Modal analysis, which was used to determine the natural frequencies of the structure. The results of Modal

analysis are presented in Table 5. The fundamental frequencies are higher than 40 Hz and pass the requirement of exceeding that value by a large margin.

Table 5: Natural frequencies of the structure

Mode	Frequency (Hz)
1	1524.5
2	1546.6
3	1578.5
4	1609.8
5	1879.8
6	1937.3

Finally, the Modal analysis results are given to two separate random vibration analysis modules (Figure 20). Power Spectrum Densities (PSD) for random vibration tests from SpaceX Falcon 9 user manual (Space X, 2021) and General Environmental Verification Standard (NASA, 2019) were used in each of those random vibration tests (Figure 20).
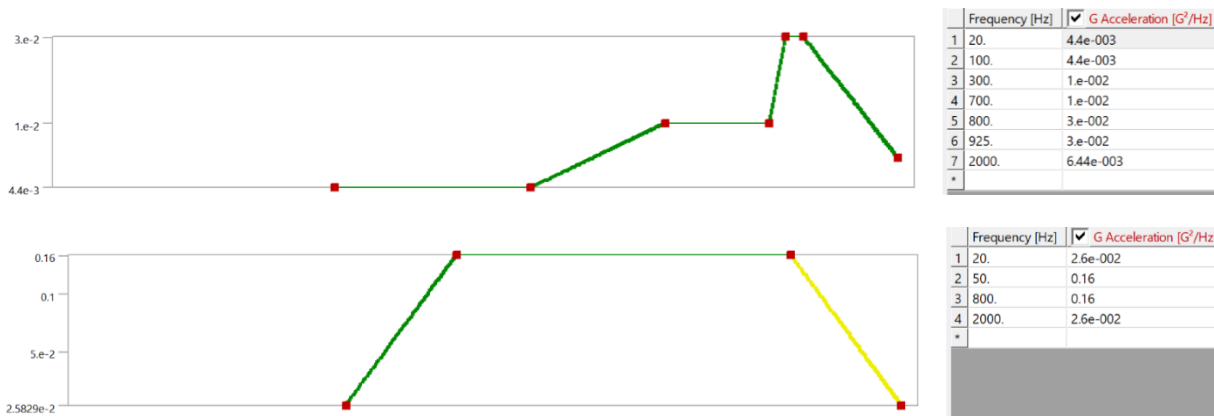
Figure 20: PSD for SpaceX Falcon 9 and NASA GEVS random vibration analyses.

The PSDs were applied to the fixed supports on the tabs in the y-direction since the mechanical subsystem is simulating the launch conditions. The deformation results and the loading on the tabs were found and confirmed to be within the requirements. Deformation experienced by the structure is insignificant, with a maximum of 0.043 mm deformation occurring during GEVS random vibrations simulation. The maximum stress also occurred in the GEVS random vibrations analysis and was 19.552 MPa which is under the allowed

503 MPa. When it comes to tab loading the requirement is to be under 3995 N in all directions, below in Table 6 the peak forces on the tabs are compiled. The highest loading force is lower than the limit with a safety factor of 2.8.

Table 6: Loading forces on the tabs during random vibration simulations

	GEVS	SpaceX
X-axis	244.29 N	120.01 N
Y-axis	1428.6 N	694.4 N
Z-axis	755.72 N	376.09 N

The final set up for ANSYS simulations is shown below in Figure 21. In conclusion, the analysis above demonstrates that the mechanical design of Appleton CubeSat meets all the considered requirements imposed by NASA, SpaceX Falcon 9 and Planetary System Corporation CSD. Large safety factors allow the assumption that all the requirements would still be met if a finer mesh were to be generated.
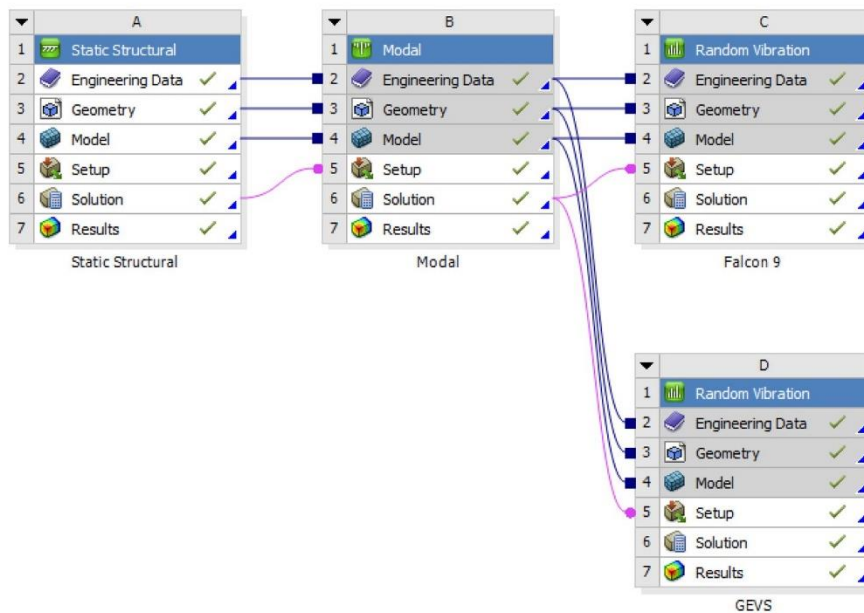
Figure 21: ANSYS Model Workbench set up

4   Power

The power subsystem will provide sufficient power to the telemetry, propulsions, payload, thermal and attitude control subsystems for the duration of the mission, will provide power with solar panels and an onboard battery, and will ensure that stored power is available for an end-of-mission deorbit. This section will describe the power subsystem design and analysis.

4.1   Power Overview

This subsystem will fulfil the following key functions; the generation, storage and distribution of power onboard the spacecraft.

The most common methods for power generation on small spacecraft are solar panel arrays, which offer the benefit of generating constant power so long as they are in direct sunlight, and onboard nuclear power cells, which offer the benefit of not needing any sort of light to use and using negligible amount of onboard fuel. As the spacecraft will be in a semi-sun-synchronous orbit around earth, with short periods of eclipse, as well as high power usage for a spacecraft of this size, solar panels are the evident choice. However, a battery will be required to power the spacecraft when in eclipse. This battery can be small as it does not need to hold power for a long time and can be recharged whenever the spacecraft is in sunlight and not using all the power that it generates.

Power generation will be conducted using deployable solar cells. These cells will be oriented on the sun facing side of the spacecraft, with an approximate beginning of life (BOL) efficiency of 29-31% and an approximate end of life (EOL) efficiency of 24-26%. However, this EOL efficiency would only occur after 10 years, given the mission lifetime of 180 days, the actual EOL efficiency will be 29 percent. The maximum power generation will be 220 watts, while maximum achievable generation will be 200 watts. Peak power generation will be impossible to always achieve due to the minor periods of earth eclipse, the non-ideal panel direction, and atmospheric interference. Power conditioning is a secondary function required as part of power

generation and will be conducted using a power conditioning unit. This will optimize the output of each solar panel as well as ensure that the failure of a single panel will not result in the loss of all power to the CubeSat. This optimization is due to the relation that as current draw increases, voltage will decrease.

Power storage will be conducted using a battery. This battery will be used to store excess power for use during eclipse, and will start the mission fully charged, or near full charge. It may not be fully charged if that is unobtainable due to factors such as the CubeSat being put in extended storage. For the mission duration, with the exceptions of initial deployment and deorbit, the battery is not to exceed a depth of discharge of over 30% to extend battery life. Were this not possible the battery's maximum stored power would be lowered with each charge and discharge. Additionally, to prevent damage to the battery, it must be kept above a certain temperature. This will be achieved with a built-in heater. Given the heat maintained by the thermal subsystem being –20 degrees Celsius, relatively minimal heating should be required to maintain the required temperature.

Lastly, power distribution will supply power at the appropriate current and voltage to the other subsystems and monitors current draw. This will be conducted with a power distribution unit and a power management unit. These will provide the appropriate current and voltage to each subsystem.

4.2 Power Component Selection

Component selection is based on all available constraints, specifically this section will focus on spatial constraints inside of the dynamic envelope as well as the power supply constraints applied by the power needs of the other subsystems. After these constraints are addressed, components will be sorted based on their mass, volume, reliability, synergy, and lifetime.

The first component to be selected is the solar panel array. This array needs to be able to fulfill the power budget needs of the spacecraft. Efficiencies between different panel types typically vary only by 1-2 percent; however, the thickness can vary significantly from panel to panel. A thinner panel will reduce the stowed volume and possibly lend itself to more efficient folding, resulting in a larger surface area after

deployment. The thinnest available panel that has been found is the Solareo ZTJ series. With a beginning of life efficiency of 29.5%, an end-of-life efficiency of 25.2%, this panel will generate the most power in an array based on out physical constraints and will be capable of subsequently filling the current and projected power constraints. Furthermore, this panel has a low mass, with a solar cell mass of $84g/cm^2$, has a high degree of reliability, fulfilling the industry quality standards, and an acceptable lifetime, this lifetime being 10 years, an order of magnitude longer than out mission (SolAero, 2018).

The second component to be selected is the battery. Of the batteries identified as meeting the available space and power storage requirements, the Clyde space battery, the Optimus 40 to be ideal. Specifically, this battery was chosen because it is part of a set, simplifying use and fulfilling the synergy section of selection, the mass is higher than that of some other similar battery systems, such as the ISISpace MPS, however, the greater degree of reliability caused us to make this selection. All of these batteries are lithium polymer, preferred due to the higher reliability than other batteries such as lithium Ion, even at the cost of the lowered energy density (AAC Clyde Space, 2019).

The final piece to be chosen, the power distribution and power management chosen was the Starbuck Nano Plus. It fulfills the space requirements given and synergizes well with the battery as they are made by the same manufacturer. This power conditioning unit offers the following power outputs; 3.3 V, 5 V, and 12 V. Additionally, this product offers a high degree of inbuilt utility that would otherwise require the purchase of more parts and lead to potential compatibility issues.

The completed power system diagram is included below, with the following subsystems connected to the different buses: The 3-volt bus powers the command and data handling subsystem as well as the payload, the 5-volt bus powers the attitude control subsystem, and the 12-volt bus powers the telemetry subsystem and the propulsion subsystem.
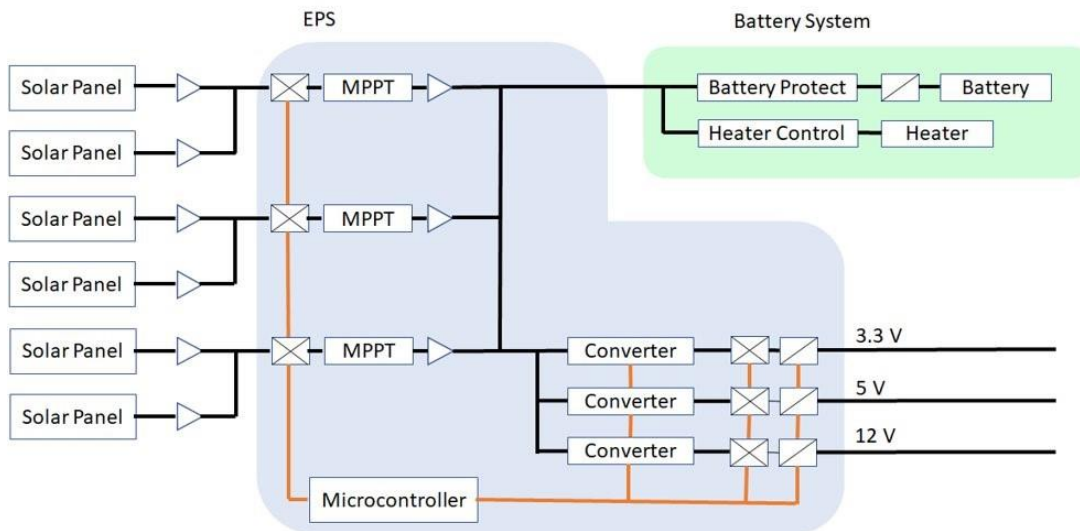
Figure 22: Power Subsystem Diagram

As you can see above, six solar panels leading into the EPS passing through current and voltage sensors into three MPPTs. These solar panels are bound into groups of two with diodes to ensure proper current flow in the event of power imbalance. The MPPT ensures that maximum power is generated. The EPS is wired to the battery system, which is comprised of a battery protector, a heater, a switch, and the battery. Power will flow into the battery when there is a power surplus or will be switched to flow out of it when there is insufficient power. Either the battery is powering the spacecraft, or the solar panels are, the EPS is not set up in such a way that power could be drawn from both at once. The microcontroller then converts the power into three buses that the other subsystems are then connected to.

4.3   Solar Panel Geometry

Several factors were considered for panel geometry. Firstly, the power subsystem needed to maximize surface area, given the dynamic envelope of the dispenser and that each panel is 2 mm thick, this allowed stack three panels to be stacked on the top and bottom faces of the spacecraft.

This mission will make use of an articulated panel design. A stack of three panels will be located on the nadir and anti-nadir sides of the spacecraft, specifically the two be three U sides. These will fold out parallel to

the one by two U side facing the sun. This will allow us to maximize surface area while minimizing the chance of a shadow being cast on the panels by the body of the spacecraft.

Two panel folding configurations were considered. The power subsystem first considered folding the panels up, and then having one emerge from the left and one from the right as depicted below:
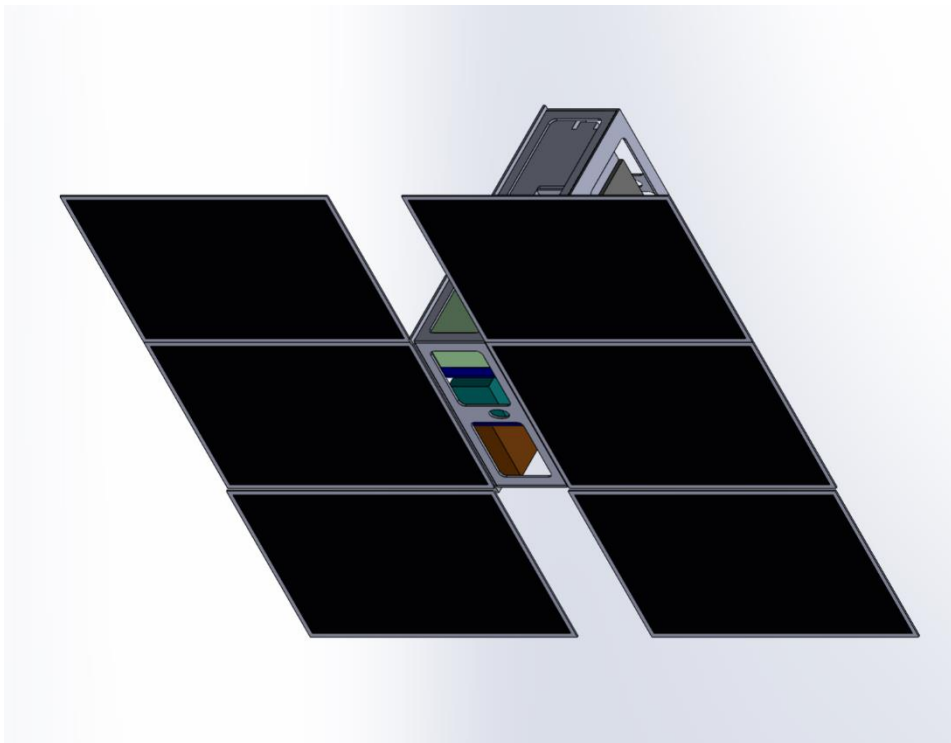
Figure 23: Initial Solar Panel Configuration

The other panel configuration that was considered, and the one that was decided on was an in-line panel design where all panels will fold out in line with each other. The power team decided to use this configuration due to ease of use and so as not to interfere with the sunlight sensors located on the faces of the CubeSat. This design is depicted in Figure 18, depicted again here for ease of reference.
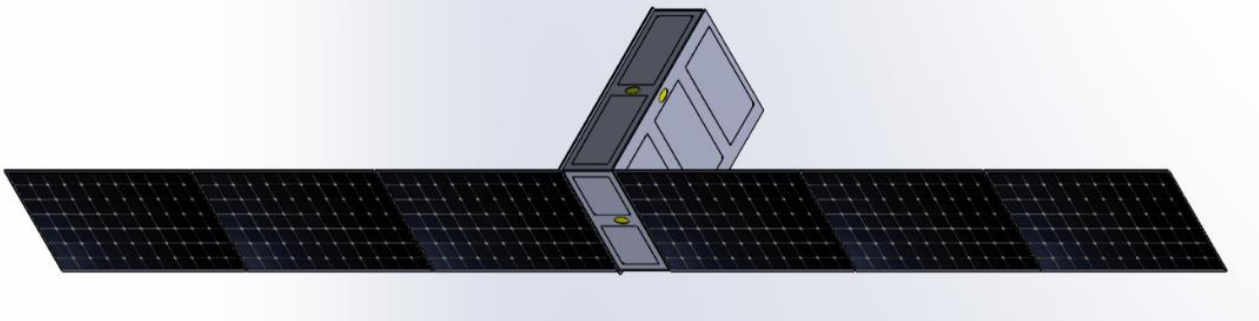
Figure 24: Final Solar Panel Configuration

4.4 Solar Power Generation Modeling

This analysis used STK and MATLAB to model the power generation of each mission leg. First, a simulation was run in STK which determined the maximum power that could be generated by the panels for the dull duration of each leg. This table was then plugged into a MATLAB program that compared the power use of the spacecraft to the power generation to find when the panels produced sufficient power and when the spacecraft would need to resort to using its battery. An array was kept of the power stored in the battery over time considering the discharge from battery use and the recharge when the panels were being used. The STK scenario that was used is noted in 5.4, the Orbital Analysis section. This task was important as the spacecraft can never be allowed to run out of power, as with no backup power supply it would become unresponsive, ceasing to collect data or perform station keeping, resulting in a premature deorbit.

4.5 Solar Power Analysis

For power generation modeling the power team modified an existing spacecraft, adjusting the size of the solar panels to fit the actual planned panel size. This .mdl file was downloaded from an STK tutorial, where following the tutorial, the panel models were manually resized by opening the .mdl file as a text document and altering the values defining panel size. This model was then imported into the scenario provided by the propulsion subsystem,

STK's solar panel tool uses the following equation to determine the power output of the satellite.

$$P = n * A * G * \cos(\theta) * I$$

Where *P* is the power output of the solar panels, *n* is the panel collection efficiency, *A* is solar panel area, *G* is solar flux, *θ* is solar incidence angle, and *I* is irradiance. These were double checked by hand using all the inputs provided by STK to ensure that there were no errors caused by mis-sizing of the components. This analysis uses an efficiency of 30% based on the expected beginning of life efficiency and the low percentage of the component lifetime used. Solar array area and solar incidence angle are used to calculate the effective solar area, that is the area normal to the Sun vector. Lastly, solar irradiance indicates the degree of obstruction from the earth, the atmosphere and any other potential obstruction that might occur over the course of the orbit. This tool provides an accurate estimation of the wattage produced by the spacecraft's solar array.

4.6 Solar Power Results

Using the STK solar panel tool, 180 days simulated with a sampling rate of one sample per sixty seconds. Several dates were then selected after this, where a sampling rate of one sample per 10 seconds was used to ensure that no data was lost due to poor resolution. The selected dates include the first and last day of the mission lifetime, in addition to any irregularities such as brief periods of eclipse. These graphs are provided below.
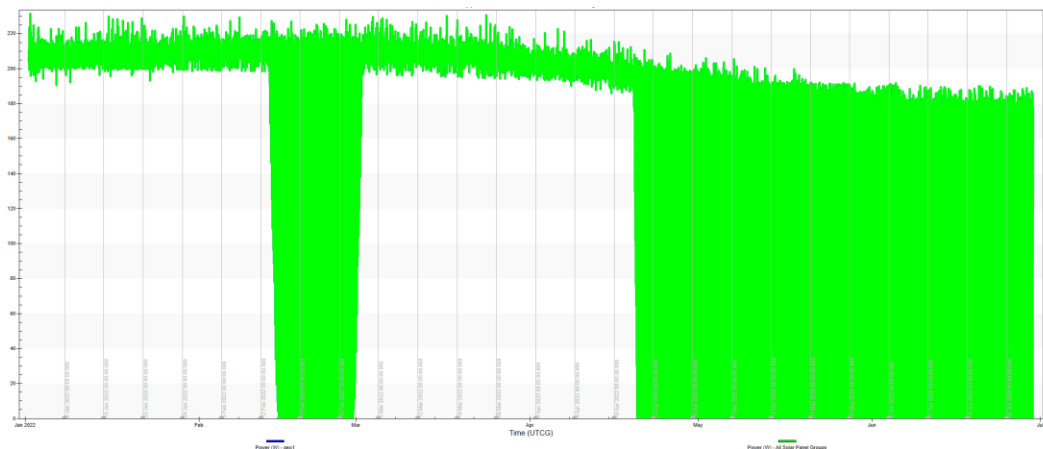
Figure 25: Solar Panel Power Mission Duration

Figure 25 indicated the power generated by the spacecraft for the entirety of the mission duration. Sections where the bar is filled in indicate periodic eclipse. Where this is not the case there is no eclipse
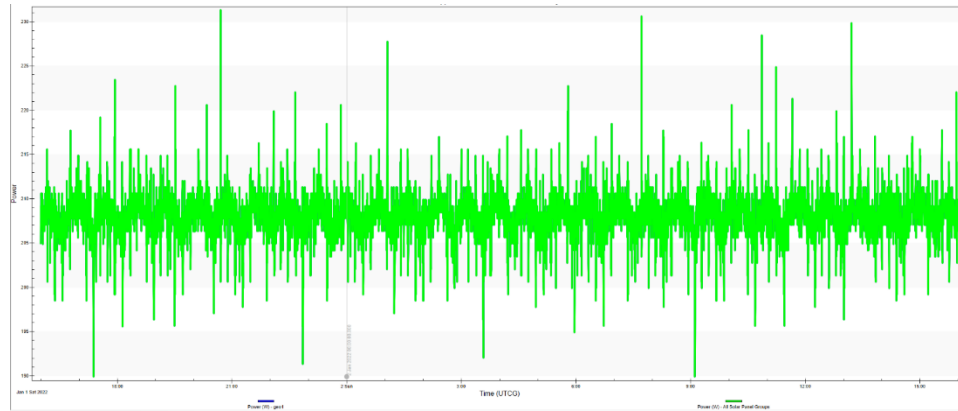
Figure 26: Solar Panel Power Over Time (January First)
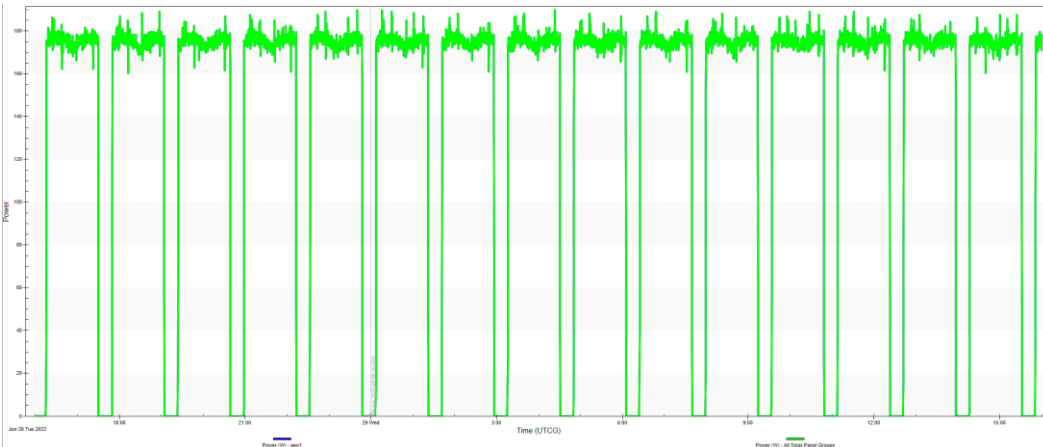
Figure 27: Solar Panel Power Over Time (June 29)
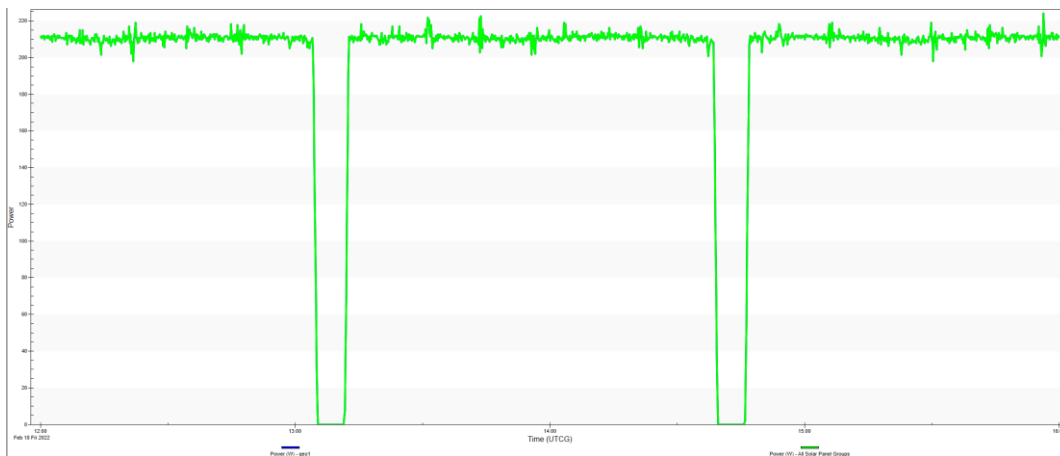
Figure 28: Solar Panel Power Over Time (February 18)

For clarity, Figure 26 is the first day, Figure 27 is the last and darkest day, having both the longest eclipses and the worst panel angle, and Figure 28 is a tighter view of the anomaly in February. The eclipse periods observed here are significantly shorter than in June.

The difficulties experienced by the propulsion subsystem team left the power subsystem without inputs on orbits, and without information on the wattage or type of propulsion system used during the solar panel geometry planning and modeling sections of the project. This led to potentially oversized panels to ensure the highest chance of successfully powering the propulsion subsystem for the duration of the mission. Even when power generation is at its lowest in June, the power generated while in sunlight is 180 watts.

Due to the semi-sun-synchronous nature of the orbit, the exposure of the panels is inconsistent over the mission duration, with both periods of time where the spacecraft regularly passes into eclipse as well as extended periods of time where no eclipse occurs. As you can see above, there are no interruptions and a constant high power input in the early months of the year. This dips down to the lowest maximum power around June, where there are also frequent eclipses. While there are also frequent eclipses in both February and December, those are not so consequential as the periods of eclipse are far shorter. This is poorly illustrated by the full mission graph but is far better shown in the higher resolution graphs taken during June as compared to the one from February.

4.7   Dynamic Power Model

The STK simulation data is used by a Matlab program in conjunction with projected power use data to analyze the power generation and results. This program then creates a dynamics simulation, accounting for the two aforementioned factors as well as tracking battery charge. This can be used to ensure that sufficient battery power will always be available.

4.8   Dynamic Power Model Analysis

The dynamic power model predicts power use over time and compares it to simulated power generation. The propulsion and science legs are calculated separately, though station keeping burns are factored into the power use data of the science leg as all other processes continue uninterrupted. This simulation runs for the full 180-day mission time before checking on battery status for deorbit.

Due to the high degree of redundancy in the power subsystem some conservative assumptions are made about the power use of other subsystems in order to ensure continued functionality of the spacecraft should it be found that the predicted power use was not accurate. The attitude control system will be assumed to always be functioning at full power, which while not realistic will ensure that the subsystem is never in danger of drawing too much power. The telemetry subsystem will be assumed to be permanently operating at full power as well.

All power demands are small relative to the power generated by the solar arrays. In June, at the lowest power generation per day, the panels produce approximately 180 watts. The propulsion subsystem uses 65 watts, the telemetry system uses 13 W, the payloads use 2.3 W, and the attitude control system uses 2.8 watts. A total of 83.1 watts can be drawn by turning everything on at once, as happens during station keeping, and during this there are 80 watts remaining to charge the battery.

This is then used to determine the maximum number of panels that could fail while still letting the spacecraft function for the full mission duration. This is done by assuming that in the event of collision or other failure pairs of panels will totally fail. If one panel ceases to function its MPPT partner will also work at a dramatically reduced efficiency. As it cannot be determined exactly what this is this section will assume the worst-case scenario, which would be nothing. With the loss of one third of the power generation capacity, the minimum power generation would dip to 120 watts. Here is the full subsystem power use table:

Subsystem	Peak Wattage
Telemetry	13
Propulsion	65
Payload	2.3
Attitude Control	2.8
Total	**83.1**

4.9   Dynamic Power Model Results

A single analysis was conducted with the model for the full mission duration to ensure that the batteries never fully drained. The resolution of this simulation was 60 seconds. This larger simulation was followed by several smaller simulations each run over the course of 24 hours with a resolution of 10 second, which is the maximum that can be achieved from the higher resolution data taken by the shorter time frame STK simulations.

Three station keeping burns are conducted over the course of the mission, each lasting for three days, all system function remained normal for this time. These are the times when power failure becomes a threat to the mission.

During the first leg of the mission, power generation constantly sits around 210 watts, with a variance of three watts. During this stage of the mission the batteries will not be used at all, even in the result of one third of the panels being damaged.

During the science leg of the mission the only substantial danger is power failure during eclipse. Therefore, to test the capacity of the spacecraft the power this simulation was run on the worst day of the lifetime, with the lowest power generation and the longest eclipse. Here is the graph:
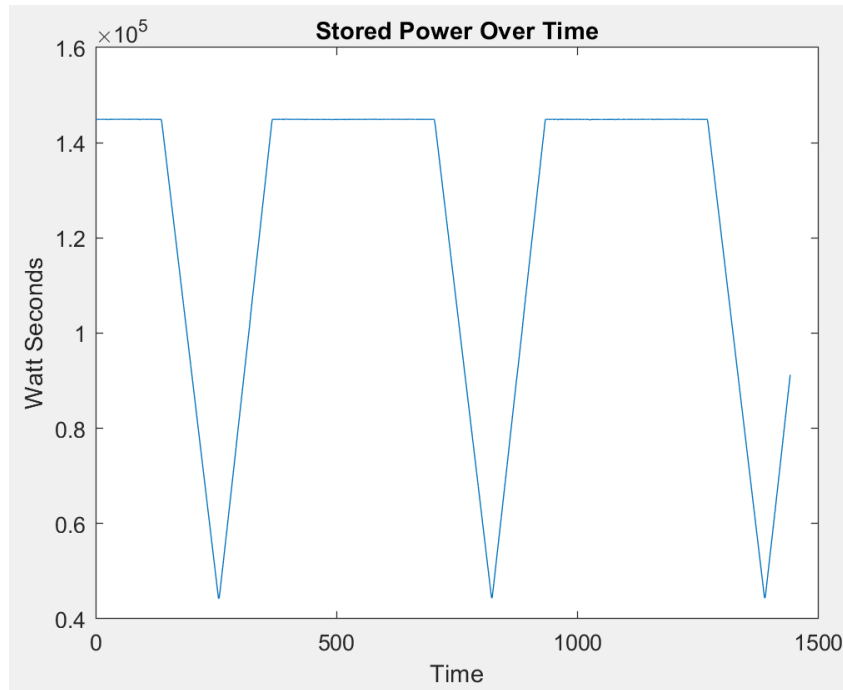
Figure 29: Store Power over time (June 29th)

As you can see, the graph assumes that the spacecraft is undergoing station keeping as well as transmitting data, meaning that it is at maximum power draw. Despite this the subsystem does not run out of power during periods of eclipse and quickly restores the battery's full capacity. For additional clarity, the time scale is in tens of seconds.

It will be impossible to store sufficient battery power for a controlled deorbit due to the insufficient maximum power capacity of the battery. The battery, while fully charged, could only power the propulsion subsystem for less than an hour. However, given the decreased power consumption during the deorbit phase, periods of eclipse of up to 40 minutes can be endured without running out of power. So long as deorbit can be ensured before the periods of eclipse become too long, deorbit is achievable.

There are two ways that the power subsystem could fail. Firstly, the power generated could be under the power expenditure, or the spacecraft could run out of stored power during a period of eclipse. As mentioned previously, redundancy was provided in the power subsystem. Given the maximum power consumption coming in at 83.1 watts, and the lowest power generation coming in at 180 watts, for a period of one hour of sunlight

between eclipses, the power surplus generated is 96.9 watts. This means that one third of the power generation could go down while still providing sufficient power for the spacecraft. However, if power generation were reduced by two thirds, power generation would be 60 watts, while would be insufficient for station keeping maneuvers. However, if station keeping were halted Appleton would still be able to continue its mission with a power surplus of 42 watts. Secondly, Given the one-hour timeframe for the batteries to recharge, and the maximum battery capacity of 40 watt hours, that means that the battery needs an excess of 40 watts for the during the period of power generation to ensure that power failure does not occur during eclipse. Should one solar array fail, resulting in the loss of one third of the total generated power during station keeping, the power surplus would fall to 36.9 watts, which is just under what is required to fully charge the battery from nothing, however, given the maximum of a 20-minute periods of eclipse while using 83.1 watts, only 27.7-watt hours would be used, still allowing the spacecraft to be recharged fully. Should two thirds of the power generation be lost, station keeping would need to be abandoned in order to generate a surplus. However, the total number of watt hours needed would fall to six watt hours, meaning that only a six surplus would need to be maintained to avoid power failure. As mentioned above, in this case there would be a 40 watt excess, ensure the mission could still be completed. However, controlled deorbit would become impossible as thrusters could only be fired for 40 minutes before power failure due to the capacity of the battery.

5 Propulsion

The purpose of this chapter is to present information regarding the propulsion subsystem of the Appleton CubeSat mission. The discussion will be focused on the development and analysis of the orbital model used for mission design, as well as the propulsion system selection process.

5.1 Propulsion Overview

The propulsion subsystem is responsible for performing orbital transfers and maintenance throughout the duration of the mission. For the previous MQPs which included a dedicated analysis of the propulsion subsystem, the project objectives were like this team's, yet the scope was limited in comparison to the Appleton mission. These missions required less resource-intensive transfers to final orbits with less eccentricity than those required for the mission (A. Brown et al., 2021), (Clavijo et al., 2020). As such, the initial thruster selection process for the Appleton mission was larger in scope due to the added propulsive requirements. The projects do share similarities in the framework of analysis for the propulsion subsystem. Initial research was focused on determining the orbital maneuvers required to achieve mission objectives, followed by a trade study of propulsion systems that met the mechanical and power constraints. From this initial study, and using estimates for the orbital transfer requirements, a more refined selection of thrusters was considered. These thrusters were then analyzed in their effectiveness and efficiency in achieving the desired orbital transfer and mission lifetime. From these results, a final thruster could be selected and further modeled to ensure effectiveness.

5.2 Thruster Trade Study

Due to the nature of the mission, including the outlined eLEO orbit into the ionosphere and the desire to utilize the propulsion system to counteract drag forces, there were several imposed requirements during system

selection. Any propulsion systems that would be considered must be compact in dimension and low in total mass due to limitations in the CubeSat size. Based upon the volume requirements of the GRIDS and INMS, as well as other subsystems, the propulsion system was confined to a volume of 1018.38 cm³. This includes the volume available to the thruster body, its components, and the propellant tank. It also must have a bus power requirement of less than 120W due to the maximum power available as set by the power subsystem. Finally, it must be able to effectively complete the orbital transfer required while still having enough propellant to extend the mission lifetime with station-keeping maneuvers. This means the thruster should also have a high thrust-to-power ratio to maximize the ΔV possible given the limited power supply and a high specific impulse to minimize propellant consumption. As shown later in the orbital analysis, the thrust must also be capable of multiple start-stop operations.

With these considerations in mind, a trade study was conducted consisting of research in a variety of propulsion types. The first propulsion type considered were liquid monopropellant thrusters. The only variety of chemical thrusters considered, monopropellant thrusters eliminate the need for an oxidizer system by containing the oxidizing agent and combustible matter within a single fluid (Sutton, G.P. et al., 2017). This reduces the tank volume required, as all liquid can be stored within a singular tank. It also makes the mechanical design of the system simpler, as there are a reduced number of tubes and valves required when compared to bipropellant systems. Due to the propellant's nature to yield combustion gas when heated or catalyzed, these thrusters rely on a catalyst bed to decompose the propellant and produce an exhaust gas that can be expelled to produce thrust. This type of thruster can be expected to have a thrust capability of 0.05 to 0.5N with specific impulse values ranging from 150 to 225 seconds (Sutton, G.P. et al., 2017). Busek's BGT-X5 Green Monopropellant Thruster was considered a representative model for this class of propulsion. Having a nominal thrust of 0.5N and a specific impulse of 225 seconds, its parameters are at the higher end of most monopropellant thrusters of this size (Busek, 2021). It also utilizes an ASCENT green propellant which is more stable, environmentally friendly and has a 45% higher density than hydrazine, which is the industry standard. This stability simplifies tank

storage and reduces transportation costs significantly. The system meets the constraints set by the mechanical and power subsystems as well, as it only operates on a system power of 20W and requires 1U of volume. Finally, another benefit of the BGT-X5 is its capability of start-stop procedures, allowing for more complex orbital maneuvers.

Table 8: BGT-X5 Green Monopropellant Thrust Characteristics (Busek, 2021)

System Power	20 W
System Volume	10cm x 10cm x 10cm
System Mass	1.5 kg
Propellant Type	ASCENT
Nominal Thrust	0.5 N
Specific Impulse	225 seconds
Total Impulse	565 N-s

The next propulsion type considered were electrostatic thrusters. This includes Ion thrusters and Hall Effect thrusters. Although similar, these propulsion types have a few notable differences. Ion thrusters usually consist of three main components: a plasma generator, accelerator grids, and a neutralizer cathode. By ionizing a large fraction of its easily ionized and high atomic mass propellant, usually through methods such as electron bombardment, biased grids can electrostatically extract ions from this plasma and accelerate them to high velocities (Goebel, D. M. et al., 2008). This process of accelerating and expelling ions is what creates thrust. Hall Effect thrusters accelerate these ions in a different manner. Instead of utilizing grids to extract and accelerate ions, Hall thrusters establish an electric field perpendicular to an applied magnetic field to electrostatically accelerate ions to high exhaust velocities (Goebel, D. M. et al., 2008). There are also three main components of these thrusters: the cathode, the discharge region, and the magnetic field generator. Electrons expelled from the cathode tend to spiral around the thruster axis due to the induced magnetic field from coils

around the thruster. As these electrons travel, they collide with the expelled gas (often xenon) from the anode and create ions, which are then accelerated by the electric field and are expelled to create thrust. Typical Ion thrusters have thrust capabilities within the range of 0.005mN and 0.5N and specific impulses within 2000 to 6000 seconds (Sutton, G.P. et al., 2017). Hall Thrusters are similar, although they can achieve higher thrust to power levels at the cost of lower specific impulse values. They range from 0.005mN to 0.1N of thrust and 1500 to 2500 seconds for specific impulse (Sutton, G.P. et al., 2017).

ThrustMe's NPT-30 I2 Smart Iodine Electric Propulsion System was chosen as the representative model for Ion propulsion technology. Capable of 1.1mN of thrust and a specific impulse of 2400 seconds, this thruster has respectable performance values for an ion thruster of its size (ThrustMe, 2021). The draws to this thruster are in its modular design and propellant type. Housing the thruster body as well as its PPU, feed system, propellant tank, and thermal management system within its 1U configuration, the NPT is mechanically efficient. This efficiency is added upon by its usage of solid iodine propellant. Iodine has a higher density than xenon, 4.9 kg/L compared to 1.66 kg/L, allowing for greater fuel storage and therefore more capability within a smaller volume. This fuel also does not need to be pressurized during launch, improving vehicle safety. It is far within the range of allowable system power requirements, only requiring 65W at max operating power, and can operate start-stop operations and be continuously throttled.

Table 9: NPT-30 I2 Thrust Characteristics (ThrustMe, 2021)

System Power	65 W
System Volume	9.6cm x 9.6cm x 11.3cm
System Mass	1.2 kg (including propellant)
Propellant Type	Iodine
Nominal Thrust	1.1 mN
Specific Impulse	2400 seconds

Total Impulse	5500 N-s

The other electrostatic thruster considered for the trade study was the Busek BHT-100 Hall Thruster. Offering higher thrust but lower specific impulse than the NPT030 I2, the BHT-100 can produce 7mN of thrust and operates at a specific impulse of 1000 seconds (Busek, 2021). The thruster can achieve maneuvers requiring a large ΔV due to this high thrust and total impulse. It is mechanically efficient as well, only having a main thruster volume of approximately 0.25U. Although this would allow for multiple thrusters to be housed within the spacecraft, its large power draw of 100W approaches the maximum power output Appleton is capable of, removing the possibility of a multi-unit configuration. This thruster also would require external tanks, requiring more volume within the spacecraft, and requires an external PPU and management system. The BHT does provide the option to use either xenon or iodine as the propellant, reducing this requirement.

Table 10: BHT-100 Thrust Characteristics (Busek, 2021)

System Power	100 W
System Diameter	8.0 cm
System Length	5.5 cm
System Mass	1.16 kg
Propellant Type	Xenon or Iodine
Nominal Thrust	7.0 mN
Specific Impulse	1000 seconds
Total Impulse	45360 N-s

Other thruster subtypes were not considered for this trade study for a variety of reasons. Electrospray and Pulsed Plasma Thrusters, although mechanically efficient and having high values of specific impulse, do not offer an optimal level of thrust for the maneuvers required for this mission. They are more suitable for attitude control rather than orbital transfer. Larger Hall Effect Thrusters could not be considered as well due to their power requirements exceeding what the spacecraft can provide. Other chemical thrusters such as bipropellant thrusters offer exceptional thrust, but their volume requirements are far beyond what Appleton is capable of housing. The three thrusters selected above were considered the most promising in achieving mission goals effectively and within the outlined constraints.

5.3 Initial Thruster Analysis

In order to analyze the thrusters and determine which would be used as the primary propulsion system for the Appleton mission, initial performance estimations were made using MATLAB and a mission scenario was created utilizing the Systems Tool Kit (STK). These initial calculations allowed for a further understanding of what each system was capable of, as well as providing an idea of what performance parameters would be required to successfully transfer from the initial parking orbit to the final scientific orbit. The initial calculations carried out were meant to estimate the ΔV budget required for the complete burn sequence. This estimate assumes that the burns carried out are impulsive, which when utilizing low thrust methods of propulsion is an incorrect assumption. Therefore, it is meant solely as a benchmark used to compare thruster performance. Utilizing the developed script, a ΔV budget of 539.2 m/s was calculated. This is a useful value in determining the required specific impulse needed in order to maintain a reasonable propellant mass. As shown by the Rocket Equation below, ΔV can be calculated using specific impulse.

$$\Delta V = -gIsp \ln \left(\frac{mf}{mi} \right)$$

Equation 2

It was assumed that the mass fraction would be approximately 0.75, as the maximum initial mass for our CubeSat due to the Canisterized Satellite Dispenser is 9.1 kg and the dry mass was estimated to be 6 kg when

considering payload and other subsystem components. Therefore, in order to ensure the mass was held within this constraint, total wet mass would be held to under 8 kg. From this limit, it can be determined that the minimum required specific impulse would be approximately 191.25 seconds. All three thrusters previously identified met this criterion, although the BGT-X5 was near this boundary. The next step in estimating thruster performance was to determine the ΔV budget for each individual thruster. Assuming a maximum initial mass of 8 kg, the given or estimated propellant mass was subtracted to determine the final dry mass of the spacecraft. This could be done utilizing the equation for total impulse shown below, assuming constant thrust.

$$I = M_p I_{sp} g$$

Equation 3

Utilizing **Error! Reference source not found.** and the estimated propellant mass values, the ΔV budgets for each thrust is shown in Table 11. Based on these estimations, each thruster also meets the required impulse capability to achieve the necessary ΔV budget. The BGT-X5 and NPT-30 I2 also have low propellant mass values, allowing for reduced volume constraints and higher thrust-to-weight possibilities. When using **Error! Reference source not found.** with the impulse capability in Table 10 provided for the BHT-100 thruster, the propellant mass calculated is beyond Appleton's ability to carry. A more representative fuel mass of 0.5 kg yields a ΔV capability of 634 m/s. This shows how due to the BHT-100's low specific impulse, it requires more fuel to achieve a similar ΔV to the NPT-30 thruster.

Table 11: Estimated Propellant Mass and ΔV Budget

	BGT-X5	BHT-100	NPT-30 I2
Propellant Mass	0.256 kg	4.62 kg	0.234 kg
Estimated ΔV Budget	767 m/s	8497 m/s	700 m/s

Once fuel mass is estimated, the fuel tank size can be determined. To do this, a spreadsheet was developed in which the parameters of a Ti-6Al-4V cylindrical tank could be manipulated in order to store the required fuel volume. The propellant volume was found from the estimated required propellant mass of each

thruster and the utilized propellant density. A tank safety factor of 2.0, mass factor of 1.25 (in order to include mounting and other tank components), and aspect ratio of 4.0 were maintained for all calculations. The internal radius of the tank was manipulated until the internal volume of the tank was that of the required fuel mass for each thruster as shown in Equation 4.

$$V = \frac{4}{3}\pi r^3 + AR\pi r^3$$

<div align="right">*Equation 4*</div>

Because the NPT-30 I2 is sold as a complete unit and stores the iodine propellant within its 1U frame, it was not considered necessary to include in these calculations. The results of these calculations are provided in Table 12. The estimated tank masses were determined based on the Ti-6Al-4V material density, the calculated wall thicknesses, as well as the surface areas for both the cylinder and end caps.

Table 12: Estimated Fuel Tank Sizing

	BGT-X5	BHT-100
Propellant Mass	0.256 kg	0.5 kg
Internal Radius	2.19 cm	2.55 cm
Aspect Ratio	4.0	4.0
Internal Volume	176.55 cm3	278.31 cm3
Tank Mass	0.028 kg	0.0442 kg

From these calculated values, estimated wet masses for each of the thrusters can be determined and compared. The NPT-30 is sold with a wet mass of 1.2kg, while the BGT-X5 is estimated to have a wet mass of 1.784kg. Finally, the BHT-100 was estimated to have a wet mass of 1.704kg, assuming 0.5kg of propellant is utilized. With the initial thruster parameters determined, these values could be imputed into a STK scenario in order to further analyze their effectiveness.

5.4 Orbital Analysis

The Systems Tool Kit was an invaluable tool during propulsion subsystem analysis, allowing each thruster's performance to be tested and compared in order to finalize the system chosen for the mission. This was done by developing a scenario that modeled two-stage finite transfers from Appleton's initial state post-ejection from the Falcon 9 launch vehicle to the desired final scientific orbit utilizing the various propulsion systems. Further analysis into thruster performance and capability could then be conducted. Once a thruster was determined to be most effective, transfer optimization was then focused on in order to make the orbital maneuvers as efficient as possible. The final stage of propulsion analysis centered on understanding the mission's lifetime with and without station-keeping, as a vital task of the subsystem is to maintain the scientific orbit to allow for long-duration data collection.

Table 13: Appleton Required Maneuver Summary

Phase	Maneuver	Altitude of Periapsis	Altitude of Apoapsis
Initial Orbit	N/A	625 km	625 km
Transfer Stage #1	Apogee Raise	Initial: 625 km Final: 625 km	Initial: 625 km Final: 800 km
Transfer Stage #2	Perigee Lower	Initial: 625 km Final:180 km	Initial: 800 km Final: 800 km
Science Orbit	Station-Keeping	180 km	800 +/- 50 km

5.4.1 Initial State and Parking Orbit

As discussed in Section 3.1.2, with the Falcon 9 used as the launch vehicle for the Appleton mission, the CubeSat will be ejected over a range of altitudes from 500 km to 600 km. Assuming a possible error of +/- 25 km, the maximum altitude of the initial parking orbit was 625 km. This would represent an initial state which

would require the largest change in altitude and ΔV, and therefore the largest available propellant mass. For this reason, all scenarios utilized this altitude for the initial altitudes of periapsis and apoapsis. Due to the requirement that the Appleton also has a final orbit that is semi-sun-synchronous, the orbital inclination which would be maintained throughout the mission was determined utilizing a MATLAB script. This ensured that there were limited periods without solar intensity to allow for optimal power generation. Inclination to achieve semi-sun-synchrony was determined to be 97.34 degrees. Other orbital parameters, such as the right ascension of the ascending node, argument of periapsis, and true anomaly were maintained at zero degrees.

Figure 30: Orbital Elements of the Initial State

The next step in defining the initial state was to input the characteristics of the Appleton spacecraft into the scenario. It was estimated that the final dry mass of the CubeSat was approximately 6 kg, based on the component mass of other subsystems and thruster dry mass. For drag effects, the area was calculated based on the ram-facing area of the satellite while the drag coefficient was estimated based on calculated values for CubeSats with similar cross-sections and operating altitudes (Oltrogge, D. L. et al., 2011). Solar radiation and

radiation pressure areas were calculated in similar methods, based on the area of the sun-facing side of Appleton. The remaining values for the spacecraft parameters were left in their default values, as it was assumed that they were reasonable estimates which would not create large errors within the model.

Figure 31: Spacecraft Parameters of the Initial State

The final step in defining the initial state of the scenarios was inputting the fuel tank parameters. This was done utilizing the previous calculations carried out for each of the three thrusters in Section 5.3. Fuel masses were limited to 2 kg, as with an estimated dry mass of 6 kg, a total wet mass of 8 kg was the maximum allowable mass for our 6U CubeSat. Tank sizing also limited the available propellant mass, as mechanical constraints based on the thruster body and component volume left limited space for external tanks. For tank pressure, values were inputted based on the propellant type and the thruster manufacturer recommendations. Fuel density was also based on the propellant type utilized by the thruster. For the BHT-100, which had been tested using both Xenon and Iodine, only Iodine was considered due to its higher density.

Figure 32: Fuel Tank Parameters of the Initial State

5.4.2 Apogee Raising Maneuver

Once the initial state is set and able to propagate, the first stage of the transfer is initiated to raise the

apogee altitude from 625 km to 800 km. To do so, a sequenced set of burns within a propagation segment were

initiated based on a variety of starting and stopping conditions. These burns, which would take place at the

orbital apogee for a duration based upon thrust capabilities, were triggered if, when at perigee, the altitude of

apoapsis was below 850 km. This sequence would continue until one of two stopping conditions were met. The

first was the constraint of maximum duration, ensuring that the sequence terminated after an excessive period.

The second constraint was triggered when the altitude of apoapsis reached over 850 km, stopping the sequence

at perigee and allowing the next stage to commence. 850 km was selected to be the stopping condition as the

perigee lowering maneuvers degraded the altitude of apoapsis by approximately 50 km once completed.

Therefore, in order to achieve a final orbital apogee of 800 km, this added altitude was set to account for this

degradation. Once developed, this sequence was propagated for each thruster and initial state to compare

performance. The results are shown below in Table 13.

Thruster	NPT-30 I2	BGT-X5	BHT-100
Single Burn Duration	800 Seconds	200 Seconds	600 Seconds
Total Burn Duration	96.22 Hours	0.25 Hours	17.17 Hours
Fuel Mass Used	0.016 kg	0.203 kg	0.044 kg
ΔV Achieved	61.21 m/s	69.27 m/s	66.78 m/s

These results reveal the various strengths and weaknesses for each thruster. Due to the NPT-30's high specific impulse, it can achieve the required ΔV without using a large amount of propellant compared to the other thrusters. This is ideal for CubeSat missions in which the mass and volume constraints are strict. The drawback of this thruster is its lower nominal thrust, reducing the ΔV of each maneuver and therefore requiring a long duration to complete the first stage of the transfer. For the Appleton mission, this is not a major concern as there is not a constraint for the data collection start time, therefore more emphasis is placed on reducing the power and mechanical requirements for the propulsion subsystem. The BGT-X5 juxtaposes the NPT-30's performance, as its high thrust capability allows for low burn duration and therefore faster transfers. The issue with monopropellant thrusters of this nature is their low specific impulse, meaning the BGT-X5 uses a large amount of propellant to complete this transfer. The BHT-100 thruster's performance is more balanced, as its specific impulse and thrust capability allows it to complete the transfer faster than the NPT-30 while using less propellant than the BGT-X5. The main drawback for the BHT-100 thruster is its large bus power requirement, making optimal performance conditions difficult to achieve and maintain.

5.4.3 Perigee Lowering Maneuver

After achieving the desired final altitude of apoapsis, the next stage of the transfer seeks to lower the perigee altitude from 625 km to 180 km to achieve the eccentricity of the desired final orbit. This was completed in a similar manner to the first stage of the transfer, utilizing a sequenced set of burns with

constraints to starting and stopping conditions. For this sequence, burns of varying durations based upon thruster capability are initiated at the periapsis of the orbit. These maneuvers are triggered based on if, when Appleton is at apoapsis, the altitude of periapsis is greater than 180 km. This sequence is allowed to continue until one of the following stopping conditions are triggered. The first, like the initial stage, is a set maximum duration ensuring the sequence concludes if the thruster is unable to complete the transfer. The second stops the propagation once the altitude of periapsis is below 180 km. After this sequence is completed, the Appleton CubeSat will have reached its final orbit of approximately 180 km by 800 km, an eccentricity of 0.633. Once developed, the final stage of the transfer sequence was propagated for each thruster to compare performance, as shown below in Table 14.

Table 14: Stage-Two Periapsis Burn Results

Thruster	NPT-30 I2	BGT-X5	BHT-100
Single Burn Duration	800 Seconds	200 Seconds	600 Seconds
Total Burn Duration	197.78 Hours	0.42 Hours	29.83 Hours
Fuel Mass Used	0.033 kg	0.339 kg	0.077 kg
ΔV Achieved	126.30 m/s	121.35 m/s	117.15 m/s

5.4.4 Full Transfer Results

Once both the apogee is raised to 800 km and the perigee is lowered to the final 180 km, the transfer segment of the mission is complete. Figure 33 below shows the changes in apoapsis and periapsis altitude over the duration of the transfer for each thruster.
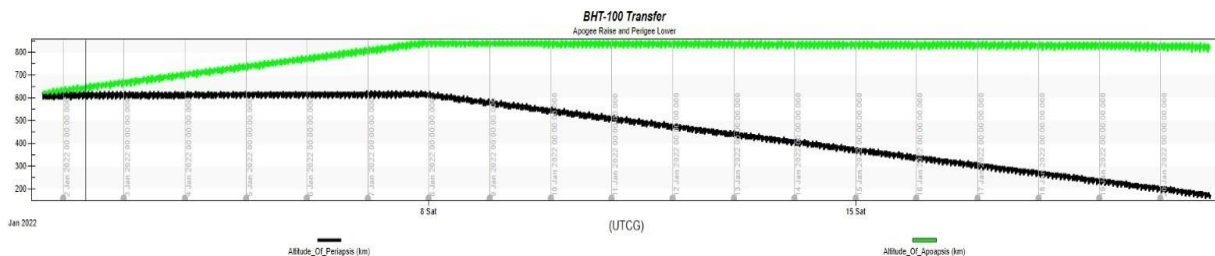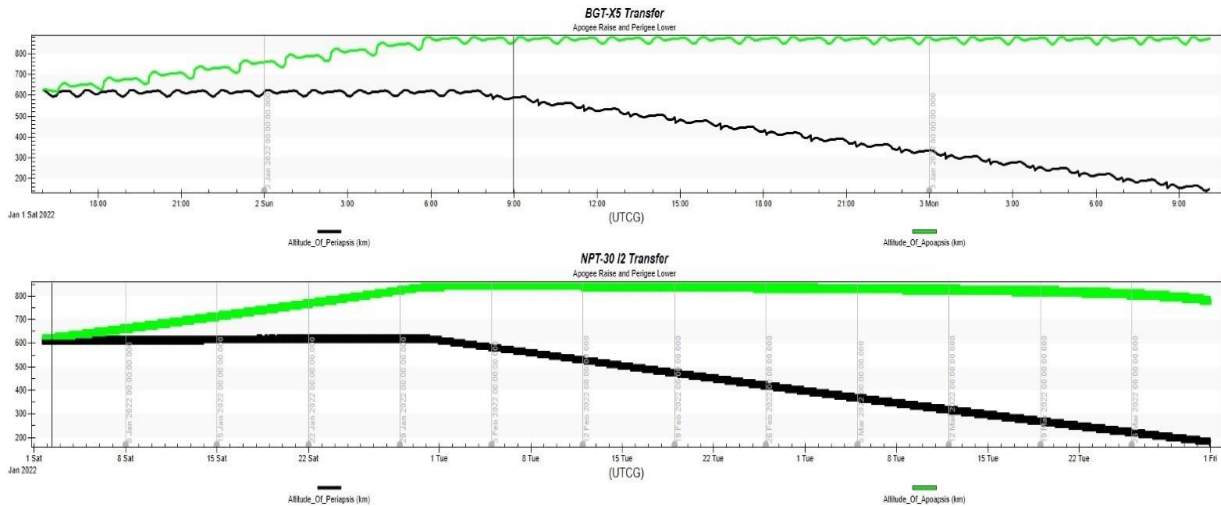
Figure 33: Changes in Altitude During Transfer Sequence

After completing the transfer analysis, it was decided that the BGT-X5 would not be considered as a possible thruster system any longer. As expected for a monopropellant thruster, its low specific impulse creates a propellant requirement that cannot be met by the Appleton CubeSat. In order to complete the transfer, a fuel mass of 0.542 kg was required. With a fuel density of 1.45 g/L, this means that the volume required to store the propellant would be approximately 380 cubic centimeters. This added to the 1U thruster body, would far exceed the volume constraints provided by the mechanical subsystem. Therefore, for the later stages of the propulsion analysis, only the NPT-30 and BHT-100 thrusters would be considered.

Table 15: Transfer Maneuver Results

Thruster	NPT-30 I2	BGT-X5	BHT-100
Total Burn Duration	12.25 Days	0.028 Days	1.96 Days
Transfer Duration	~90 Days	~1 Day	~20 Days
Fuel Mass Used	0.049 kg	0.542 kg	0.121 kg
Fuel Mass Remaining	0.185 kg	0.008 kg	0.379 kg
ΔV Achieved	187.51 m/s	190.62 m/s	183.93 m/s

The performance of these two thrusters after the two-stage transfer is well within the mechanical constraints of Appleton. The NPT-30 used 21% of its fuel mass to complete the transfer while the BHT-100 exceeded this by using 24% of its propellant. Although the BHT-100 will require utilize far more propellant than the NPT-30, its small thruster volume allows for over 700 cubic centimeters of propellant storage. This value may be smaller due to the unknown volume of the external thruster components such as the PPU, but when only storing 0.5 kg of fuel with a volume of 278.31 cubic centimeters it is assumed to be within mechanical constraints. The largest difference between the two thrusters is in the total transfer duration. The BHT-100 can complete both stages of the transfer 4.5 times faster than the NPT-30 due to its superior thrust capabilities, which has the drawback of requiring far more power than the less taxing NPT.

5.4.5 Station-Keeping Maneuvers

Although the main requirement of the Appleton propulsion system was to achieve the final scientific orbit, it was also necessary to demonstrate the importance of having a thruster capable of extending the mission lifetime. The station-keeping analysis is the final stage of the propulsion system analysis, showing how the NPT-30 and BHT-100 perform when attempting to counteract orbital perturbations and increase mission duration. The first stage of this analysis was to determine the mission lifetime without any intervention from the propulsion system post-transfer. Using the Lifetime Analysis tool in STK and an initial state of the final scientific orbit, it was determined that deorbit would occur 69 days after the transfer orbit finalized. This value would be compared to the data collection duration of sequences which utilized station-keeping maneuvers. The next stage was to develop a sequence in which burns would be triggered in order to maintain the scientific orbit. The main constraint which would begin station-keeping maneuvers was the altitude of apoapsis. If this altitude were to drop below 800 km, then station-keeping burns would occur each orbit at apogee until altitude was raised to 850 km. Orbital perturbations such as drag would degrade the apogee over time and cause this sequence to occur again. For the purposes of determining thruster capabilities, these maneuvers would be triggered until all the fuel mass remaining post-transfer was expelled, in which the sequence would end, and the

CubeSat would deorbit. Due to the different thrust capabilities, it was determined that the NPT would burn for 900 seconds each maneuver while the BHT would fire for 800 seconds. The results of the station-keeping analysis are shown below in Table 16.

Table 16: Station-Keeping Maneuver Results

Thruster	NPT-30 I2	BHT-100
Total Burn Duration	58.85 Days	8.11 Days
Lifetime Extension	~345 Days	~238 Days
Deorbit Date	5/19/2023	11/12/2022
Fuel Mass Used	0.185 kg	0.379 kg
ΔV Achieved	898.95 m/s	784.86 m/s

These entire sequences from initial parking orbit to deorbit with station-keeping maneuvers can be seen in Figure 34 below, with the X-axis representing time and the Y-axis representing altitude. The green segment of the graph shows the variation in apoapsis altitude while the black is the periapsis altitude over time. From Figure 34, one can see the transfer maneuvers on the far left, followed by the oscillating pattern of the station-keeping maneuvers. This stage of the mission takes up the largest duration. Finally, on the far right of the figure, perigee and apogee altitudes decay and cause deorbit due to the spacecraft running out of propellant. Due to the NPT-30's higher specific impulse, it was better able to extend mission duration through a larger number of maneuvers due to greater fuel efficiency. With the transfer and station-keeping analysis completed, a selection could be made to finalize which thruster system will be used for the Appleton mission.
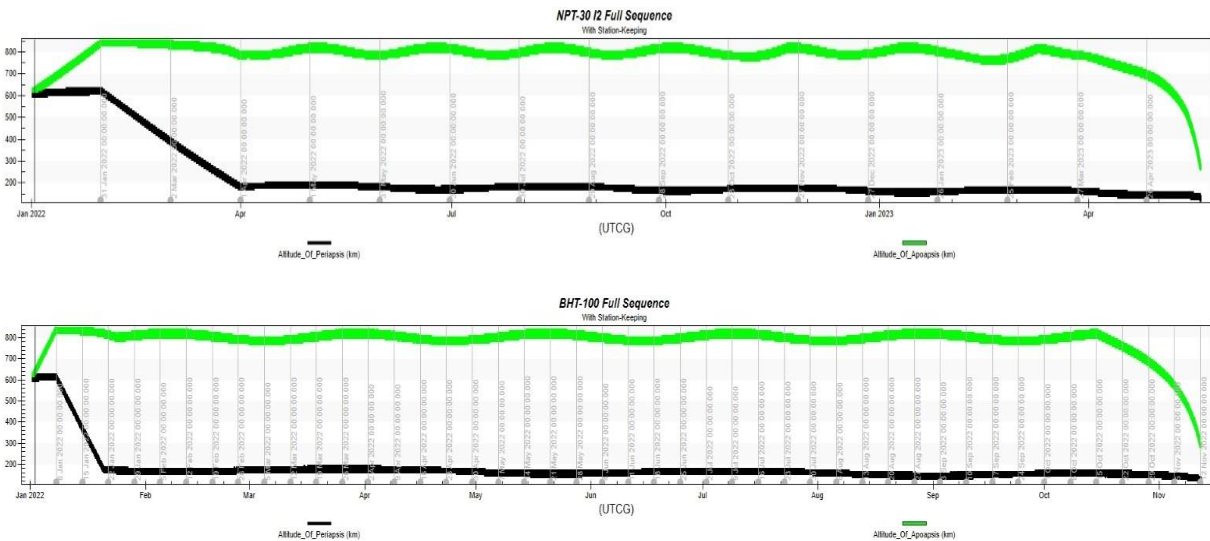
Figure 34: Full Sequence Changes in Altitude

5.5   Propulsion System Selection

After developing the two-stage transfer model and analyzing thruster performance, it was determined the NPT-30 I2 thruster would be most effective in achieving the Appleton mission's objectives under the inherent constraints. The BHT-100 thruster was also determined to meet mission requirements but was not chosen to be on the Appleton mission due to its large bus power requirement and lower lifetime extension capabilities. The NPT-30's main strength is its ability to achieve the ΔV required to reach the final scientific orbit while being within the set mechanical and power constraints of the mission. The important factors in its selection were its 1U modular design, low bus power requirement, and high specific impulse. The modular design met the mechanical constraints and removed the need for any external components, including a fuel tank of PPU. This reduced mechanical complexity and limited opportunities for a malfunction during the mission. Its pre-stored high-density iodine propellant does not require pressurization during storage or launch, improving safety and lowering propellant storage volume. The low bus power requirement of the system is beneficial as it reduces stress on the power subsystem, allowing optimal operating conditions to be maintained easily and continued performance in sub-optimal situations. Finally, the high specific impulse capability reduces fuel consumption

and allows for greater data collection durations when used to counteract orbital perturbations. For these reasons, the NPT-30 I2 thruster was selected as the main propulsion system of the Appleton CubeSat.

Table 18: NPT-30 Mission Maneuver Summary

Maneuver	ΔV Achieved	Propellant Mass Used	Altitude of Periapsis	Altitude of Apoapsis
Apogee Raise	61.21 m/s	0.016 kg	Initial: 625 km Final: 625 km	Initial: 625 km Final: 800 km
Perigee Lower	126.30 m/s	0.033 kg	Initial: 625 km Final:180 km	Initial: 800 km Final: 800 km
Station-Keeping	898.95 m/s	0.185 kg	180 km	800 +/- 50 km
TOTAL	1086.46 m/s	0.234 kg	N/A	N/A

6   Helmholtz Cage

The following section contains the current design and plans for the development of a functional Helmholtz cage to be used in ground tests of the ADCS. The method for magnetic field generation using the current design and the addition of potential air bearing platforms is discussed.

6.1   Past Project Work

A Helmholtz cage is the invention of German scientist and philosopher Hermann von Helmholtz (1821-1894). The cage consists of a pair of coils parallel to one another with each coil containing several windings. By running a current through these coil pairs, a magnetic field is created and amplified by the coil pair at the midpoint between them. The current Helmholtz cage structure and design is the result of the 2020-21 WPI MQP for the "Design of a NanoSat for an Ionospheric Mission" (A. Brown et al., 2021). The cage is made of three orthogonal coil pairs, mounted such that each pair can generate a magnetic field along a certain axis. The coil pairs are square and measure 1.44 m in length, the apparatus is shown in Figure 35. The manual for the assembly of the Helmholtz cage is in Appendix B: Helmholtz Cage Booklet.
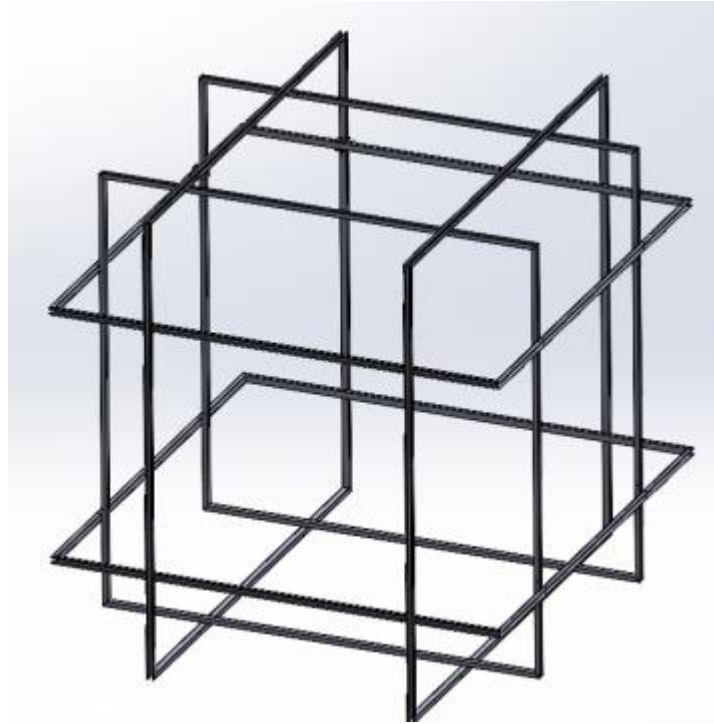
Figure 35: Helmholtz cage design (A. Brown et al., 2021)

To accurately simulate the magnetic environment of the CubeSat it was required that the magnetic field remain within 1% of the required field strength within a 0.25 m^3 volume at the center of the cage. The strength of the magnetic field across this volume was predicted using the Biot-Savart law is the unit vector of the distance between the wire element and a point within the magnetic field. Using this law, the previous team was able to create a 2-Dimensional plot showing the magnetic field strength relative to the desired value along the centerline of a single coil pair, this is shown in Figure 36.
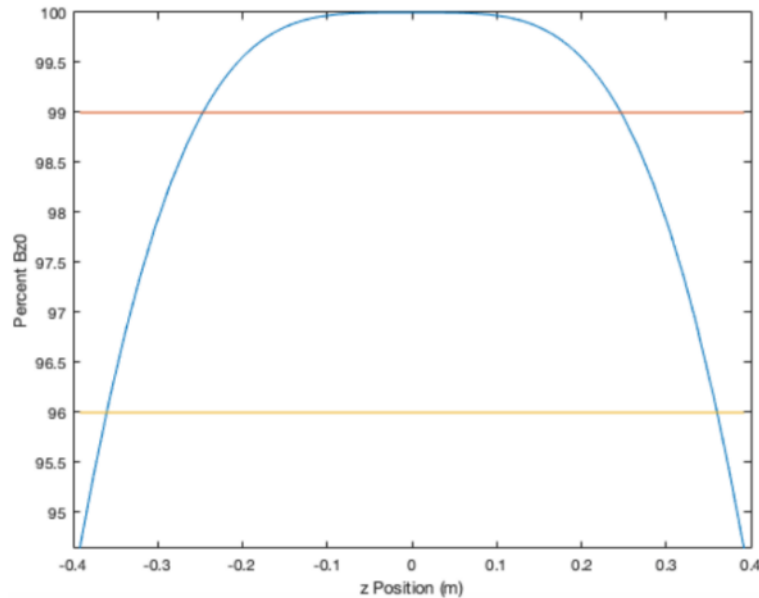
Figure 36: Helmholtz magnetic field strength along the centerline for a single coil pair (A. Brown et al., 2021)

After the construction of the cage a validation of the magnetic generation capabilities was necessary. To do this the previous team used Cytron 30A, 5-30V Single Brushed DC Motor Controllers connected to the coil pairs on each axis to vary voltage, and hence the current, thereby controlling the magnetic field produced by the coils. Adafruit's LIS3MDL Triple-axis Magnetometer was attached to a test bed at the center of the 0.25 m³ test volume to measure field strength at the center-point. This magnetometer can measure magnetic fields from ±4 G to ±16 G, at data rates from 155 Hz to 1000 Hz, allowing for real-time analysis of the cage's performance. Adafruit's INA260 sensor was used to monitor the current in the magnetic coils. This sensor measures current, voltage, and power use on the high or low side, and can measure up to 36V and 15A. An Arduino MEGA 2560 was used for data acquisition and required altering of I2C addresses to prevent erroneous data being sent. This requirement was necessary due to several identical magnetometers being used. A basic procedural outline is shown below:

- Sensor readings were plotted via Python Code
- Magnetic field data for the orbit was imported from STK as a .csv file

Test Procedure:

- Power supplied directly to DC motor controllers. The controllers are varied to achieve the current corresponding to the desired magnetic field strength, related via the Biot-Savart law.

- Current through the coils is monitored via the INA260 sensor.

- Magnetometer data is received by the DAQ (Arduino MEGA 2560) and plotted via python code over the test duration.

- The resulting plot is then superimposed over a plot of the desired magnetic field to show the strength achieved relative to the desired.
   - Note that the magnetometer only measures field strength at a SINGLE point within the cage

The program was run for approximately 50 minutes of the 60 total minutes of data. To ensure the magnetic field generation and measurements were not affected, the cage structure was not touched during the testing process. Following the completion of the test, the collected magnetic field data were plotted against the desired field data as shown below in Figure 37:
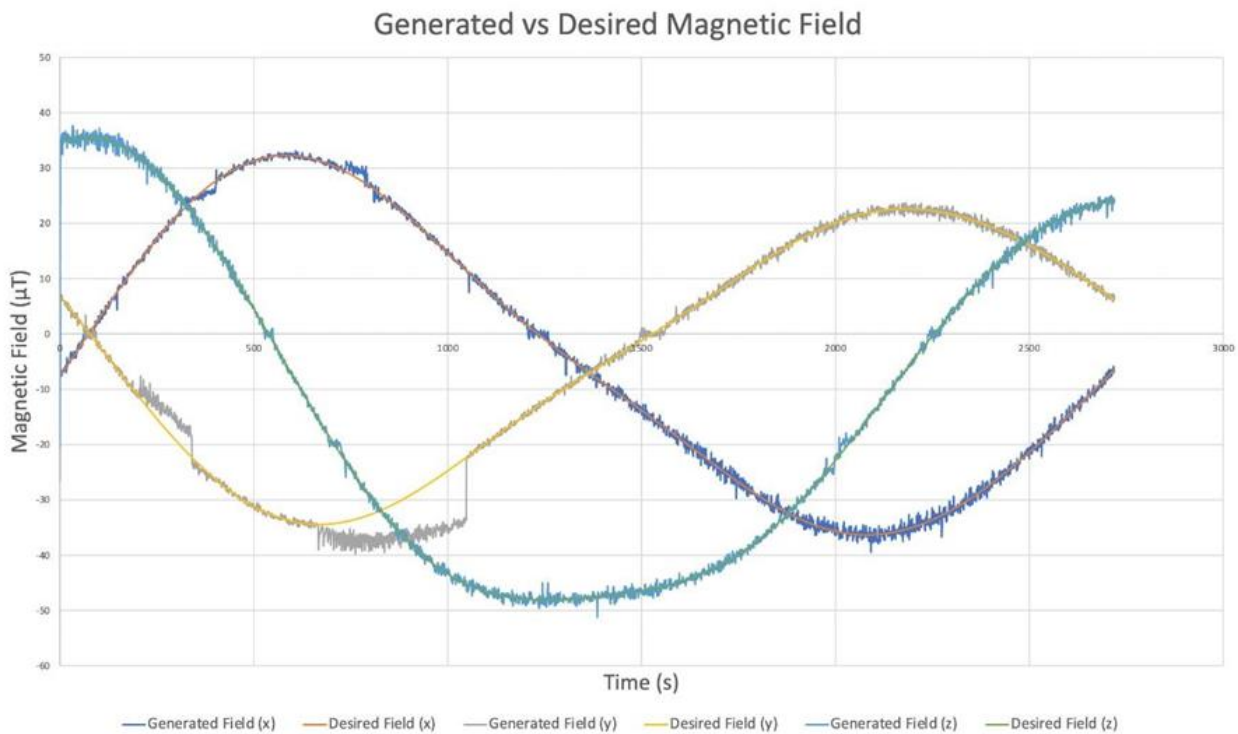
Figure 37: Helmholtz cage magnetic field test (A. Brown et al., 2021)

The data acquisition along the y-axis had the most significant discrepancy. The cause of these errors was not fully understood but was believed to be fully induced by errors in the setup of the Arduino control scheme (A. Brown et al., 2021). To improve the design, this year's team decided to move the data acquisition into a LabView based control scheme using a LabJack as a replacement for the Arduino.

6.2   Why DAQ needed to be updated

The previous Data Acquisition unit (DAQ) had several limitations that led this team to replace it. The software of this DAQ was the first limitation. First, an Arduino program must be uploaded and executed. Next, while that program ran, a python script must be started and run in parallel. The Arduino script collected and recorded the data, while the python script graphed said data. The second issue was the interaction of the scripts. The old DAQ was an Arduino unit using the Inter-Integrated Circuit (I2C) interface in connect to the Inertial Measurement Unit (IMU.) This Arduino unit took measurements from the IMU, before passing this data to the computer, where it was logged. Upon being logged by the Arduino program running on the computer, it would then be passed to a simultaneously running python script to be graphed.

This caused a problem for the recording of data, specifically, in terms of how it was passed. The Arduino code running on the computer expected to be receiving data from the IMU x times per second (where x is an independent variable.) However, data was not always being passed to said Arduino exactly when it expected it to be due to clock stretching and the maximum rate of data transfer from the IMU to the Arduino, and then from the Arduino to the computer. This led to the second problem of data not being passed correctly to the python code. Data had to be passed to the python at regular intervals, upwards of 10 times per second for the graph to be helpful. However, the python code could only read the data being passed to it at a set rate. This meant that if data were being passed too quickly it would begin skipping, resulting in occasional unrealistic numbers, or numbers including two decimal places.

Our team was able to resolve the issue of the mismatching data rates by slowing down the rate at which data was recorded from the IMU to the Arduino. However, one of this team's objectives was to integrate six additional three-axis magnetometers into the device to ensure that a uniform field strength has been achieved. Unless only a couple of readings were taken per second, it would be impossible for the existing interface to handle quadrupling the rate of data throughout, which would result in an unacceptably low resolution.

Therefore, this year's team resolved to replace the existing DAQ with a more conventional one to resolve the problems of data resolution resulting from the simultaneous scripts.

6.3   Updating Power Supplies

The previous year's project selected the Kungber variable DC power supplies to deliver power to the Helmholtz cage (A. Brown et al., 2021). Three separate power supplies were used, one power supply for each of the three pair of coils. To vary the current in each coil pair, the team used DC motor controllers. As part of the decision to integrate the Helmholtz cage into LabView, the team decided to upgrade the power supplies to the Unisource PSP-3010 Programmable DC Power Supply. The decision to upgrade the power supplies was made to remove the need for the DC motor controllers to manually change the voltage. The Unisource PSU allows the power supplies to be controlled via LabView. By integrating the PSU into LabView it will allow for a more seamless and direct control option for adjusting the coil current and therefore the coils' magnetic fields.

6.4   The I2C interface

The 3-axis magnetometers use the Inter-Integrated Circuit (I2C) interface. This means they possess a clock and data pin to transmit data to the DAQ. The lab jack is not set up the natively interpret I2C, so code will either need to be found or created in order to do that. Additionally, each I2C device has an in-built address defined by the hardware of the device. To bypass the inability to use more than one of any sensors, were have purchased and intend and intend to use a multiplexer. This multiplexer accepts inputs from several I2C devices, and then assigns them all different I2C addresses. This multiplexer should then be connected to the LabJack.

Another possibility that was explored was not using 3-axis magnetometers but instead using single axis voltage varying magnetometers. These will change their voltage depending on the strength of the magnetic field, allowing them to be directly connected to the LabJack using analog input pins. However, this is suboptimal as each magnetometer needs its own input pin on the LabJack and provides less data than its I2C counterpart.

6.5 Air Bearing Platform

To test the CubeSat ADCS, a mounting platform is required that can allow the test article torque-free motion about a single axis. In order to accomplish this an air bearing platform must be designed capable of providing enough air pressure below the test article to suspend it within the test volume. The design used in the previous MQP was an air hockey table, and due to budget limitations, the model purchased was unable to provide enough air pressure to lift any aspect of the test article (A. Brown et al., 2021). The previous air bearing platform is shown in Figure 38.

Figure 38: Air Bearing Platform from an air hockey table (A. Brown et al., 2021)

7 Conclusions, Recommendations, and Broader Impacts

7.1 Conclusions

During this project a team of eight students designed and analyzed Appleton CubeSat. In this report the focus was on mechanical design and analysis, power and propulsion subsystems. The second goal of the project was to continue developing a Helmholtz cage and air bearing system for future testing the onboard ADCS.

The Appleton Nano-Sat is a 6-unit CubeSat that is designed to orbit Earth in an elliptical semi-synchronous orbit with perigee of 180 km and apogee of 800 km. In orbit the CubeSat will begin the scientific mission of collecting data on the ionosphere using two on board payloads: the mini-INMS and GRIDS. The mini-INMS can measure densities of ions and neutral species and GRIDS calculates the total ion flux.

The mechanical design was governed by the selection of the Falcon 9 launch vehicle and a Canisterized Satellite Dispenser. The dimensions of the satellite were determined by the limitations of the CSD, while the internal structure and placement of components was done in a way that accommodated needs of all the other subsystems. The design was then analyzed using ANSYS software and verified through a series of static structural, modal and random vibrations analysis. Based on this analysis it was determined that the satellite met all the requirements set for the project.

The power subsystem part of the report focuses on the power needs for the telemetry, propulsion, payload, ADCS and thermal subsystems and ways to generate, store and distribute power to them. Six solar panels with a battery were chosen as the method to generate onboard power, a power conditioning system unit will ensure the availability of power, and power will be stored in a battery.

The propulsion subsystem part focuses on the orbital maneuvers needed to insert the CubeSat into desired orbit and maintain it. After simulating the orbit and the maneuvers in STK the propulsion subsystem selected a thruster that could provide necessary delta-V for the completion of the mission and was within power and mechanical subsystems constraints.

Finally, the report covers the process of building, coding and testing the Helmholtz cage and air bearing platform. These testing rigs are ongoing projects being built for creating desired magnetic fields and testing the ADCS in realistic flight conditions.

7.2 Recommendations for Future Work

After working on this project this team compiled several things that could have been done better, and that we'd recommend for future work

7.2.1 Integrated Systems

The team believes that should it be possible, it would be advisable to source as many parts from the same company as possible. Many companies that produce Nanosat parts produce many across the different subsystems. Sourcing from the same supplier would provide compatibility and ease of function. In addition, this would be achievable with certain suppliers.

7.2.2 Helmholtz Improvements

As noted in the Helmholtz section, the DAQ had to be replaced, along with the power supplies. Due to budgetary constraints, a LabJack was acquired to replace the old DAQ. This team recommends that should funds be available, this DAQ might be replaced with one that either integrates more easily with LabView, or with the I2C interface

7.3 Project Broader Impacts

Most spacecraft require significant resources unattainable by most non-governmental organizations. CubeSats were developed with accessibility in mind, therefore they enable a host of educational, commercial, and scientific applications with far-reaching impacts. These low-cost, compact satellites make scientific investigations and technology demonstrations in space feasible in a timely and cost-effective manner. For commercial entities, CubeSat missions allow for low-cost methods of testing new technology without the resources needed for larger-scale missions. These missions are far more time-efficient, allowing for a far more

rapid testing and development timeline. One such example is the development of MPS-130 green propellant by Aerojet Rocketdyne, which utilized CubeSats for product demonstration and testing. Other companies such as Boeing are also utilizing this design, especially when attempting to test components and subsystems in a cost-efficient method. The main purpose of the CubeSat design during its creation was to benefit educational institutions and non-profit organizations. By providing a canvas for students to actively apply their studies, these satellites have been used in a wide variety of hands-on research and problem-oriented group work for engineers. The overall societal impact of the CubeSat program is ever growing. From helping to predict storm strengths and the direction of forest fires, to testing new technology in a variety of environments, CubeSats present an array of diverse benefits and opportunities. As for the direct benefits of the success of the Appleton Mission, should the mission prove successful more information on the composition of the Ionosphere will be gained, which would be useful in several ways. Firstly, with more information on the composition of certain parts of the ionosphere, it would be possible for simulations to be more accurate, which would in turn lead to a higher chance of success for any mission relying upon it. Secondly, this higher chance for relevant mission success would also lead to a higher degree of safety for any involved crewmembers.

References

A. Brown, W. Cooley, A. Klenk, S. Messey, J. Mileti, A. Robatzek, & M. St Jean. (2021). Design of a NanoSat for an Ionospheric Mission. *WPI Major Qualifying Project (MQP) Report ZAT-2102 Advisor: Z. R. Taillefer, N.A. Gatsonis*.

AAC Clyde Space. (2019, September 1). *Optimus - AAC Clyde Space*. Https://Www.Aac-Clyde.Space/Assets/000/000/079/OPTIMUS_original.Pdf?1564954960.

Clavijo, R., Andreani, T., Joy, S., Beerbower, E., Lee, G., Valero Araujo, J., & Snyder, B. (2020). Design and Analysis of a 6U Cubesat and Mission. *Worcester Polytechnic Institute*.

Davidson, R. L., Oborn, B., Robertson, E. F., Noel, S., Earle, G. D., Green, J., & Kramer, J. (2020). The gridded retarding ion drift sensor for the petitSat cubeSat mission. *Review of Scientific Instruments*, *91*(6), 064502. https://doi.org/10.1063/1.5140470

J. Klenzing, R. L. Davidson, G. D. Earle, A. J. Halford, S. L. Jones, C. R. Martinis, N. Paschalidis, R. F. Pfaff, J. M. Smith, & K. A. Zawdie. (2019). petitSat -A 6U CubeSat to examine the link between MSTIDS and ionospheric plasma density enhancements. *AGU 100 Advanced Earth and Space Science Fall Meeting*.

J. Carnahan, & A. Kruggel. (2018). *SSC 18-IX-06 Internally Isolated 12 U Rail CubeSat Dispenser with Analyzable Boundary Conditions*. Https://Www.Semanticscholar.Org/Paper/SSC-18-IX-06-Internally-Isolated-12-U-Rail-CubeSat-Carnahan-Kruggel/73faf7eb6759264b654af1ec413e9e6b2d9c1c2b.

J. Gagnon, C. Ritter, & D. Tierney. (2022). Design and Analysis for a CubeSat Mission. WPI Major Qualifying Project (MQP) Report MAD 2022 Advisor: Z. R. Taillefer, M. A. Demetrio

J Puig -Suari, & R Nugent. (2015). *6U cubesat design specification REV*. Https://Explorers.Larc.Nasa.Gov/APMIDEX2016/MO/Pdf_files/12-6U_CDS_2016-05-19_Provisional.Pdf.

L. Keesey. (2017, May 9). *NASA Team Pursues Blobs and Bubbles with New PetitSat Mission*. Https://Www.Nasa.Gov/Feature/Goddard/2017/Nasa-Team-Pursues-Blobs-and-Bubbles-with-New-Petitsat-Mission.

Lu, Y. (2015). CubeSat Design and Attitude Control with Micro Pulsed Plasma Thrusters. *Worcester Polytechnic Institute*.

M. Hatfield. (2018, October 23). *Dellingr: The Little CubeSat That Could*. Https://Www.Nasa.Gov/Feature/Goddard/2018/Dellingr-the-Little-Cubesat-Thatcould.

M. Rodriguez, N. Paschalidis, S. Jones, E. Sittler, D. Chornay, & P. Uribe. (2016). Miniaturized Ion and Neutral Mass Spectrometer for CubeSat Atmospheric Measurements. *NASA Goddard Space Flight Center*.

NASA. (2019, April 22). *GENERAL ENVIRONMENTAL VERIFICATION STANDARD (GEVS)*. Https://Explorers.Larc.Nasa.Gov/2019APSMEX/MO/Pdf_files/Gsfc-Std-7000a_final_3-28-18.Pdf.

Nobel Prize. (2022). *The Noble Prize*. Https://Www.Nobelprize.Org/.

Olivieri, S. (2011). Modular FPGA-Based Software Defined Radio for CubeSats. *Worcester Polytechnic Institute*.

Planetary Systems Corporation. (2020). *Payload Specification for 3U, 6U and 12U*. Https://Www.Planetarysystemscorp.Com/Wp-Content/Uploads/2018/08/2002367F-Payload-Spec-for-3U-6U-12U.Pdf.

SolAero. (2018). *3rd generation triple-junction solar cell for Space Applications - Solaero Tech*. Https://Solaerotech.Com/Wp-Content/Uploads/2018/04/ZTJ-Datasheet-Updated-2018-v.1.Pdf.

Space X. (2021, September). *Rideshare payload user's guide*. Https://Storage.Googleapis.Com/Rideshare-Static/Rideshare_Payload_Users_Guide.Pdf.

T. Lizotte, H. Smith (2022). Design of a 6U CubeSat for an Ionospheric Science Mission. WPI Major Qualifying Project (MQP) Report NAG2022 Advisor: Z. R. Taillefer, N. A. Gatsonis

Appendices

Appendix A : Battery Charge Code

```
%Total Battery Charge over time
close all
clear all
clc

T = readtable('C:\Users\samaw\Downloads\ScientificOrbit_Solar_Panel_Power.csv');
%timestep = 10 seconds
Power_Gen = table2array(T(1:1443,5));
Powerdraw = 85.1;
Storedpower = 144000; % watt seconds
n = zeros(1,size(Power_Gen,1))
for c = 1:size(Power_Gen,1);
    Storedpower = Storedpower + (10*(Power_Gen(c) - Powerdraw));
    n(c) = Storedpower;
    if Storedpower > 144000
       Storedpower = 144000;
    end
end

x = 1:size(Power_Gen,1);
y = n;
plot(x,y)

title('Stored Power Over Time')
xlabel('Time')
ylabel('Watt Seconds')
```

Appendix B: Helmholtz Cage Booklet

Helmholtz Cage Instruction Manual

Recommended 2-3 people for assembly

Assembly: Outside-In Method

Frame Pairs:

NO and JOE = Inner vertical frame (X axis)

FRED and TED = Outside vertical frame (Y axis)

SMOL and PAUL = inner horizontal frame (Z axis)

NOTE: *Make sure to orient the coils so the plugs are closest to the power supply.*

NOTE: *For each pair make sure the arrows on the coil frame go the same direction.*

NOTE: *Each mounting bracket has two different sides, one with holes 5/8" from the edge of the bracket, and one with holes 3/8" from the edge of the bracket. Make sure to mount using the correct side of the brackets so the holes align correctly.*

Frame Assembly:

1. Attach brackets facing inwards on FRED and TED with pins.

2. Attach brackets facing inward on NO and JOE with pins, make sure to use the holes furthest from the corners.

Figure 39: NO and JOE

3. Stand NO and JOE up with the brackets on the two vertical sides.

4. Slot in either PAUL or SMOL between the bottom brackets of NO and JOE, secure with pins. Note:

One bracket connection for SMOL has an 'S' on it and matches a customed bracket also labeled with an

'S'.
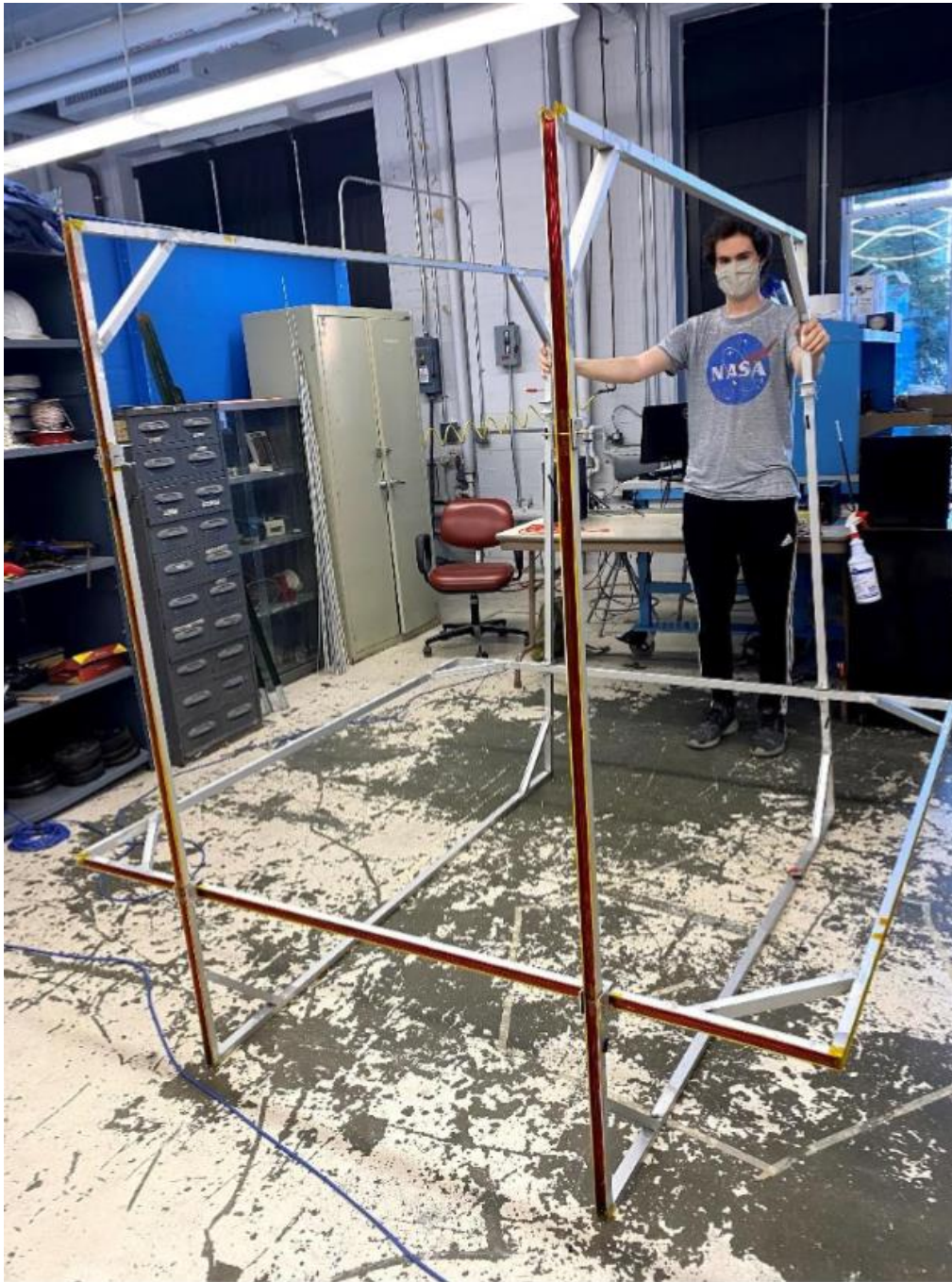
Figure 40: PAUL or SMOL connected to NO and JOE

5. Slot in either PAUL or SMOL (whichever is left) between the top brackets of NO and JOE, secure with pins.
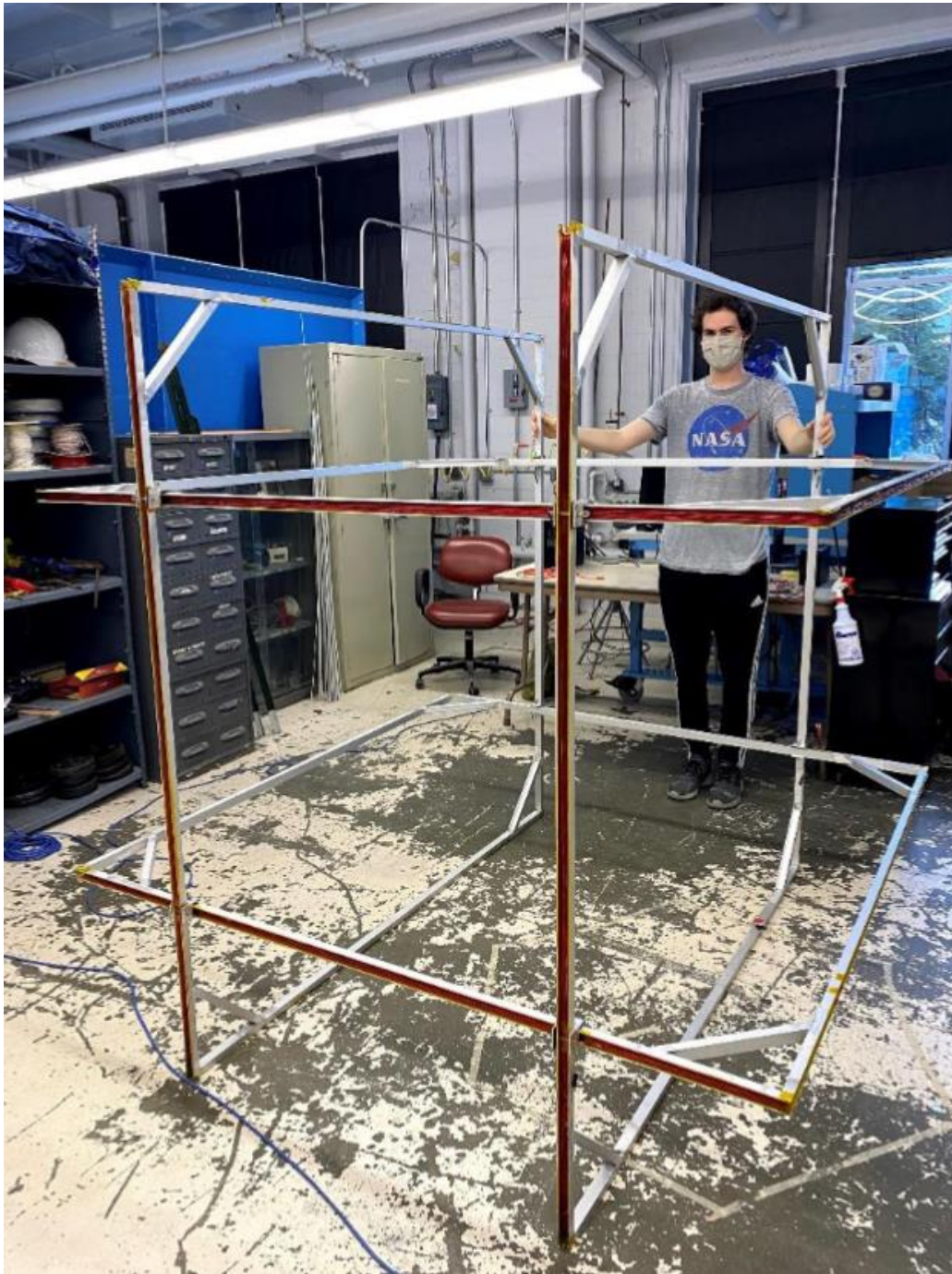
Figure 41: SMOL and PAUL connected to NO and JOE

6. Stand FRED or TED up with the brackets on the top and bottom.

7. Slightly lift the already connected frame and slide FRED or TED onto NO and JOE, secure with

pins.

Figure 42: FRED or TED added to frame

Repeat steps 6 and 7 for the remaining coil of the pair FRED and TED.
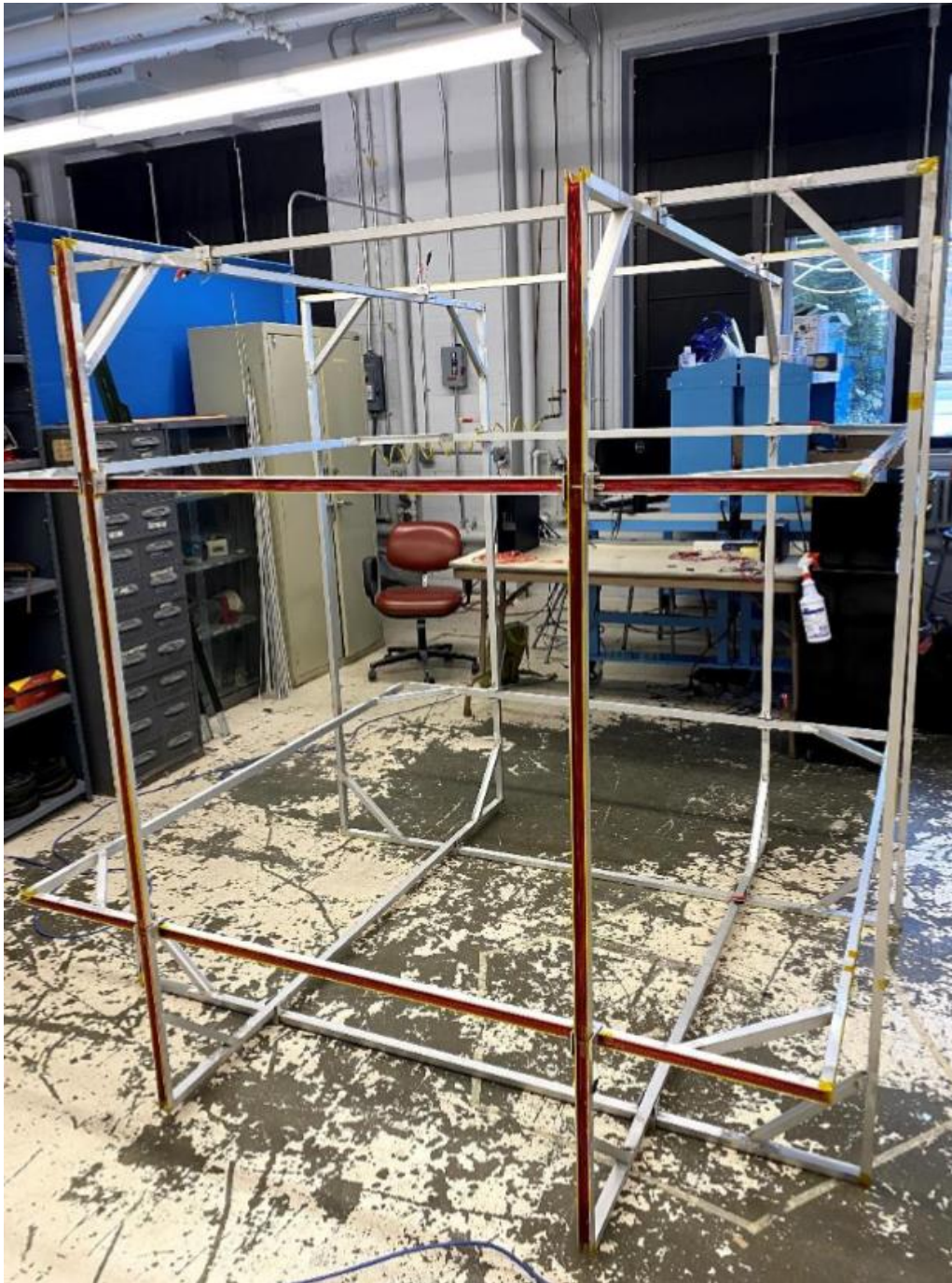
Figure 43: Full frame assembly

9. Slot the loose rubber pieces into the spaces of the brackets between the coils.

Figure 44: Bracket and rubber pieces

Connection Set-Up:

1. Connect labeled banana plug cables to corresponding coil plugs.

2. Connect the other ends of the cables for each coil pair to their corresponding splitter, based on the previously stated criteria.

NOTE: *If coil arrow directions are opposite when assembled, attach one side as red-red and black-black and the other side as red-black and black-red.*
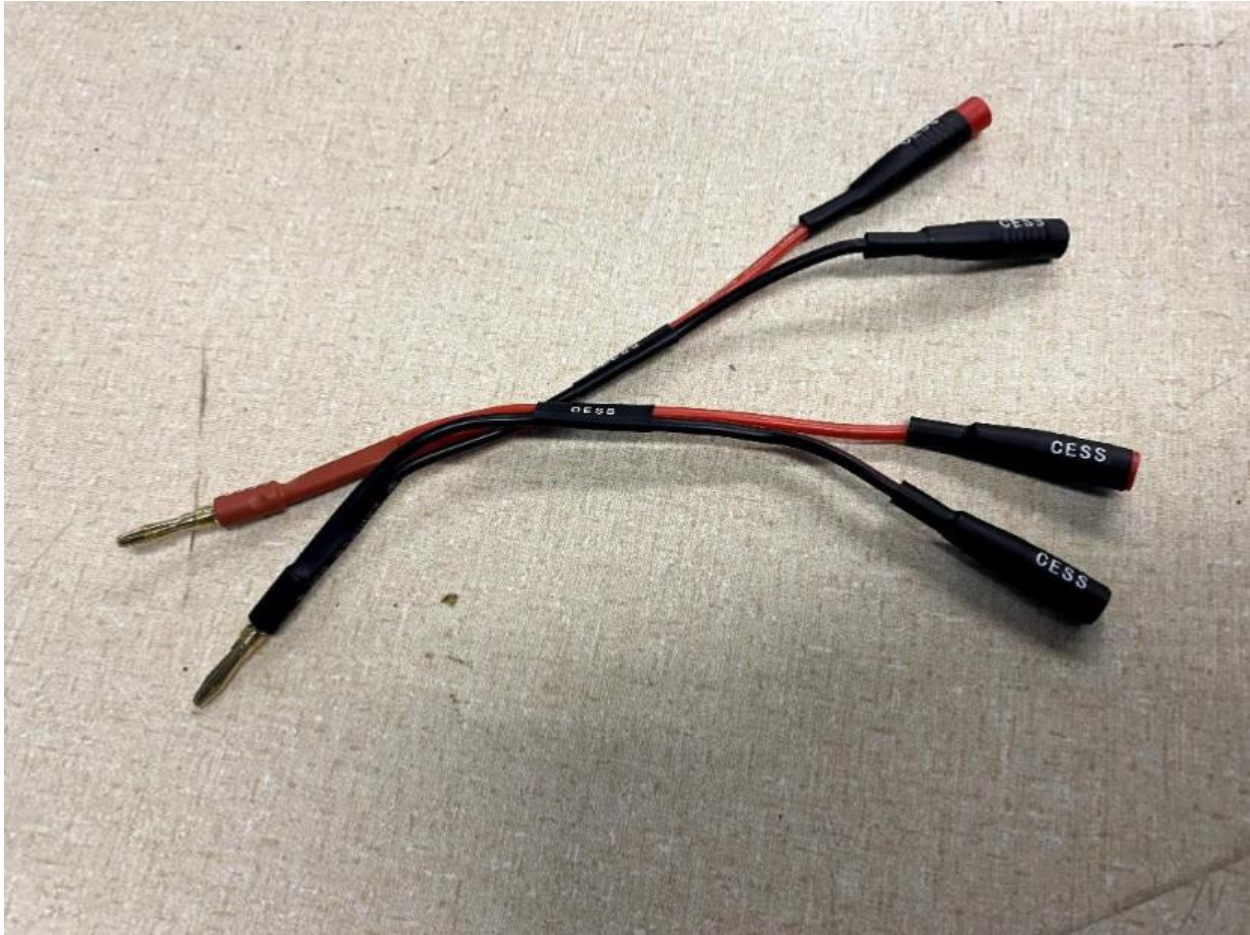
Figure 45: Splitter

LabJack/LabView integration:

To be able to interact with LabJack with or without the use of LabView several steps need to be taken. To control LabJack directly from the computer:

1. An appropriate driver needs to be installed. This driver can be found by searching "U3 Quickstart for Windows Overview".

2. Once the software package is installed the user will gain access to the LabJack control panel. LabJack Control Panel can communicate with LabJack connected via a USB, it allows to set inputs and outputs to analog and digital on different pins and control the voltage.

To integrate LabJack into LabView:

1. LabView needs to be installed, it can be downloaded through WPI Hub.

2. LabJack uses a different driver than the one provided by National instruments, so before integrating LabJack with LabView the LabJackUD driver archive needs to be installed. This archive can be found by searching LABVIEW for UD on the LabJack website.

3. The driver comes with example scripts, which can be used to test the LabJack connection (for example, U3 Read Serial Number is a good option, since the user will be able to tell if it works properly).

4. To get a control panel of LabJack into LabView, install LabJack Utilities from Interface Innovations. This is a toolkit that allows you to set input/output types, record data and overall communicate with LabJack directly in LabView.

5. This toolkit also comes with example code. Locate the National Instruments folder in Program Files (x86), then open LABVIEW 2021 folder > examples > Interface Innovations > LabJack Utilities > Basic Periodic Data Reader.
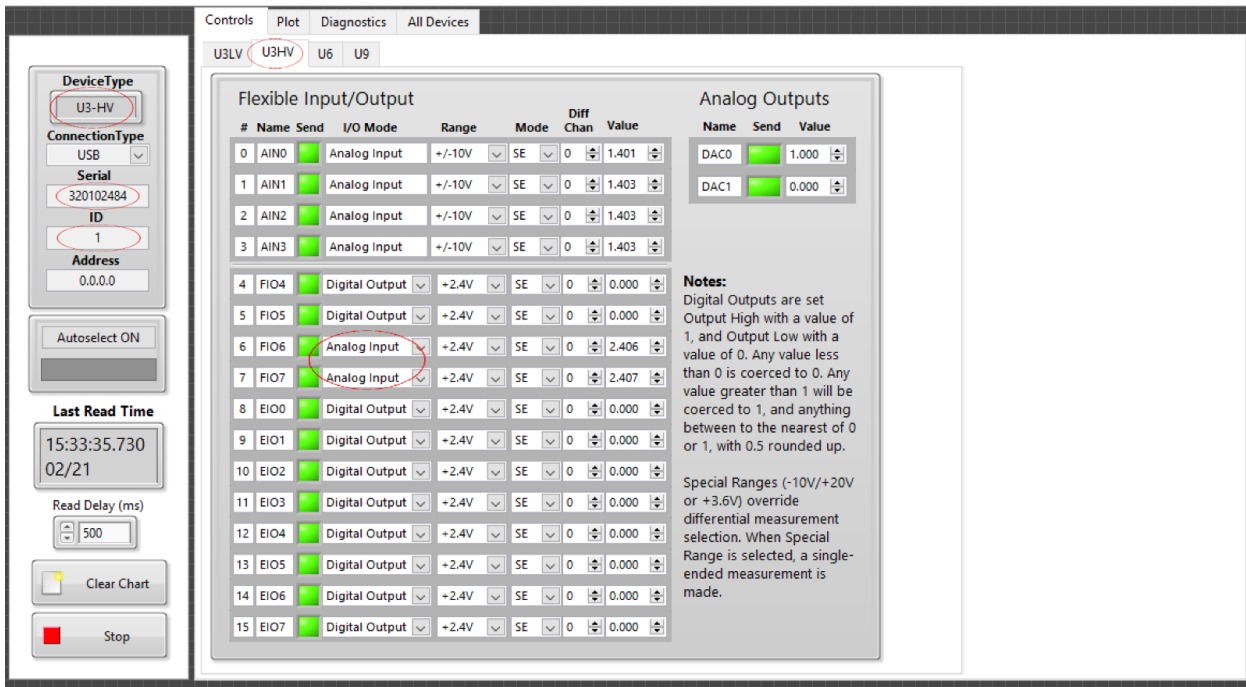
Figure 46: Labjack Controls

6. A front Panel window will open (Figure 46). Below is a screenshot of the panel, change the circled values. In the example below a magnetometer was connected to pins FIO6 and FIO7, so they were switched to Analog Inputs, a different hardware set up will require a different software set up.

7. Once the setup is complete Run the code and click the Plot tab to see data being logged

8. To modify this code open Window > Show Block Diagram, which will open the visual representation of the code behind the front panel.